CHAPTER 6

THREE-DIMENSIONAL CONTROL MODEL

6.1 Introduction

A vehicle traveling along a straight guideway can have displacements along vertical, lateral and longitudinal axes. These displacements are controlled by three Maglev technology functions — suspension, guidance and propulsion. In each dimension, there is a magnetic force to restore position and a magnetic damping force to reduce oscillations.

6.2 Vertical Position Control

The external vertical forces acting on the vehicle include the gravity force, the lift force, and the force due to random wind gusting. The initial position of the vehicle is the distance between its bottom and the ground level, which is assumed to be equal to half of the wheel diameter (1.0 ft). The vehicle takes off at the speed of 300 mph (440 ft/sec) to a desired elevation of 2.5 ft above the ground by magnetic suspension and lift force which is a function of system aerodynamic properties. Assume that vehicle remains at the desired elevation until time t = -τ sec at which wind gusting acts on the vehicle so as to effect an initial value of vertical speed.

Changes in vertical position of the vehicle over time t can be expressed by second order differential equations describing speed and acceleration due to the external forces:

$$\frac{dZ_t}{dt} = ZC_t = ZV_t \tag{6.1}$$

$$\frac{dZV_t}{dt} = ZAL_t + ZAP_t - ZAD_t \tag{6.2}$$

where Z_t = vertical position of the vehicle at time t, measured from the distance between bottom of the vehicle and the ground level (ft)

ZC_t = rate of change of vertical position of the vehicle at time t

ZV_t = vertical velocity of the vehicle at time t

ZAL_t = vertical acceleration due to lift force

ZAP_t = vertical acceleration due to levitation magnets

ZAD_t = vertical acceleration due to damping

Assuming wind force occur during a short period of time, t, and is constant, and by Newton's second law,

$$ZAW_t = \frac{WF_Z}{M} \quad , \qquad WF_Z = \begin{cases} WF_Z, & -\tau \le t < 0 \\ 0 & t \ge 0 \end{cases} \tag{6.3}$$

where ZAW_t is vertical acceleration due to wind force, WF_Z is wind force magnitude, and M is mass of the vehicle. Thus, the initial value of vertical velocity, ZVN, can be expressed in a term of wind force as:

$$ZVN = \int_0^{\tau} \frac{WF_Z}{M} dt = \frac{WF_Z}{M} \tau \tag{6.4}$$

Similarly, vertical acceleration due to lift force can be computed from the difference of lift force, LF, and weight of the vehicle, WG.

$$ZAL_t = \frac{LF - WG}{M} \tag{6.5}$$

Behaving like a spring, a set of levitation magnets create an acceleration which varies with the difference between vehicle's current position and the desired position.

$$ZAP_t = -\frac{ZK}{M} \times \left(Z_t - DZ\right) \tag{6.6}$$

where *ZK* is a suspension magnetic constant, and *DZ* is desired position of the vehicle.

A damping force, like a dashpot in a damped oscillation system, decreases acceleration as the velocity increases. The magnitude of damping force depends on a damping constant, *ZD*, supplied by a second set of magnets:

$$ZAD_t = \frac{ZD}{M} \times ZV_t \tag{6.7}$$

Substitute Equation 6.5, 6.6 and 6.7 into Equation 6.2, we obtain

$$\frac{dZV_t}{dt} = \frac{LF - WG}{M} - \frac{ZK}{M} \times \left(Z_t - DZ\right) - \frac{ZD}{M} \times ZV \tag{6.8}$$

Taking Laplace transformation of Equation 6.1 and 6.8 gives:

$$s \cdot Z(s) - ZN = ZV(s) \tag{6.9}$$

$$s \cdot ZV(s) - ZVN = \frac{LF - WG}{M \cdot s} - \frac{ZK}{M} \cdot Z(s) + \frac{ZK}{M} \cdot \frac{DZ}{s} - \frac{ZD}{M} \cdot ZV(s) \tag{6.10}$$

where *ZN* is an initial value of Z_t.

Substitute *ZV(s)* in Equation 6.9 into Equation 6.10, we get

$$s^2 \cdot Z(s) - s \cdot ZN - ZVN = \frac{LF - WG}{M \cdot s} - \frac{ZK}{M} \cdot Z(s) + \frac{ZK}{M} \cdot \frac{DZ}{s} - \frac{ZD}{M} \cdot s \cdot Z(s)$$

$$+ \frac{ZD}{M} \cdot ZN$$

$$Z(s)\left(s^2 + \frac{ZD}{M} \cdot s + \frac{ZK}{M}\right) = \left(\frac{LF - WG}{M} + \frac{ZK}{M} \cdot DZ\right)\left(\frac{1}{s}\right) + \frac{ZD}{M} \cdot ZN + s \cdot ZN + ZVN$$

Substituting natural frequency, $\omega_Z = \sqrt{\frac{ZK}{M}}$, and damping coefficient, $\alpha_Z = \frac{ZD}{2M}$, in the equation above, we obtain:

$$Z(s) = \frac{\left(\frac{LF - WG}{M} + \omega_Z^2 \cdot DZ\right)\left(\frac{1}{s}\right) + ZN\left(2\alpha_Z + s\right) + ZVN}{\left(s^2 + 2\alpha_Z \cdot s + \omega_Z^2\right)} \tag{6.11}$$

Introducing $k_Z = \frac{LF - WG}{M}$ and rearranging Equation 6.11 for the purpose of taking inverse to return to time domain,

$$Z(s) = \frac{\left(k_Z + \omega_Z^2 \cdot DZ\right)}{s \cdot \left(s^2 + 2\alpha_Z \cdot s + \omega_Z^2\right)} + \frac{ZN\left(\alpha_Z + s\right)}{\left(s^2 + 2\alpha_Z \cdot s + \omega_Z^2\right)} + \frac{\alpha_Z ZN + ZVN}{\left(s^2 + 2\alpha_Z \cdot s + \omega_Z^2\right)}$$

$$Z(s) = \frac{\left(k_Z + \omega_Z^2 \cdot DZ\right)}{s \cdot \left(s^2 + 2\alpha_Z \cdot s + \omega_Z^2\right)} + \frac{ZN\left(\alpha_Z + s\right)}{\left(s + \alpha_Z\right)^2 + \left(\omega_Z^2 - \alpha_Z^2\right)} + \frac{\left(\alpha_Z ZN + ZVN\right)}{\left(s^2 + 2\alpha_Z \cdot s + \omega_Z^2\right)} \tag{6.12}$$

A Laplace inversion of the first term can be taken utilizing the following notation,

$$L^{-1}\left(\frac{1}{s(s^2 + 2\alpha s + \omega^2)}\right) = \frac{1}{\omega^2} - \frac{e^{-\alpha t}}{\omega\sqrt{\omega^2 - \alpha^2}} \sin\left(\sqrt{\omega^2 - \alpha^2}\, t + \cos^{-1}\frac{\alpha}{\omega}\right) \tag{6.13}$$

Since

$$\sin\left(\sqrt{\omega^2 - \alpha^2}\, t + \cos^{-1}\frac{\alpha}{\omega}\right) = \sin\sqrt{\omega^2 - \alpha^2}\, t \cdot \cos\left(\cos^{-1}\frac{\alpha}{\omega}\right)$$

$$+ \cos\sqrt{\omega^2 - \alpha^2}\, t \cdot \sin\left(\cos^{-1}\frac{\alpha}{\omega}\right)$$

$$= \frac{\alpha}{\omega}\sin\sqrt{\omega^2 - \alpha^2}\,\mathrm{t} + \sqrt{1 - \left(\frac{\alpha}{\omega}\right)^2}\cos\sqrt{\omega^2 - \alpha^2}\,\mathrm{t}$$

$$\sin\left(\sqrt{\omega^2-\alpha^2}\,t+\cos^{-1}\frac{\alpha}{\omega}\right)=\frac{\alpha}{\omega}\sin\sqrt{\omega^2-\alpha^2}\,t+\frac{\sqrt{\omega^2-\alpha^2}}{\omega}\cos\sqrt{\omega^2-\alpha^2}\,t \quad (6.14)$$

Substituting the value from (6.14) into (6.13)

$$L^{-1}\left(\frac{1}{s\left(s^2+2\alpha s+\omega^2\right)}\right)=\frac{1}{\omega^2}-\frac{e^{-\alpha t}}{\omega\sqrt{\omega^2-\alpha^2}}\left(\frac{\alpha}{\omega}\sin\sqrt{\omega^2-\alpha^2}\,t\right.$$

$$\left.+\frac{\sqrt{\omega^2-\alpha^2}}{\omega}\cos\sqrt{\omega^2-\alpha^2}\,t\right)$$

$$L^{-1}\left(\frac{1}{s\left(s^2+2\alpha s+\omega^2\right)}\right)=\frac{1}{\omega^2}-\frac{e^{-\alpha t}}{\omega^2}\left(\frac{\alpha\sin\sqrt{\omega^2-\alpha^2}\,t}{\sqrt{\omega^2-\alpha^2}}+\cos\sqrt{\omega^2-\alpha^2}\,t\right) \quad (6.15)$$

Therefore,

$$L^{-1}\left(\frac{\left(k_Z+\omega_Z^2\cdot DZ\right)}{s\left(s^2+2\alpha_Z\cdot s+\omega_Z^2\right)}\right)=DZ+\frac{k_Z}{\omega_Z{}^2}-\left(DZ+\frac{k_Z}{\omega_Z{}^2}\right)e^{-\alpha_Z t}\left(\frac{\alpha_Z\sin\sqrt{\omega_Z^2-\alpha_Z^2}\,t}{\sqrt{\omega_Z^2-\alpha_Z^2}}\right.$$

$$\left.+\cos\sqrt{\omega_Z^2-\alpha_Z^2}\,t\right) \quad (6.16)$$

An inverse Laplace transform of the second term in (6.12) may be obtained by employing the following theorem:

$$L^{-1}\left(\frac{s+x}{(s+x)^2+y^2}\right)=e^{-xt}\cos yt \quad (6.17)$$

Thus,

$$L^{-1}\left(\frac{ZN(\alpha_Z+s)}{(s+\alpha_Z)^2+(\omega_Z^2-\alpha_Z^2)}\right)=ZNe^{-\alpha_Z t}\cos\sqrt{\omega_Z^2-\alpha_Z^2}\,t \quad (6.18)$$

Finally, an inverse Laplace transform of the last term in (6.12) can be determined by:

$$L^{-1}\left(\frac{1}{\left(s^2+2\alpha s+\omega^2\right)}\right)=\frac{e^{-\alpha t}}{\sqrt{\omega^2-\alpha^2}}\sin\sqrt{\omega^2-\alpha^2}\,t \tag{6.19}$$

and

$$L^{-1}\left(\frac{\alpha_Z ZN+ZVN}{\left(s^2+2\alpha_Z s+{\omega_Z}^2\right)}\right)=\left(\alpha_Z ZN+ZVN\right)\frac{e^{-\alpha_Z t}}{\sqrt{\omega_Z^2-\alpha_Z^2}}\sin\sqrt{\omega_Z^2-\alpha_Z^2}\,t \tag{6.20}$$

Substituting (6.16), (6.18), and (6.20) into (6.12) returns the vertical position in time domain, Z_t, as:

$$Z_t=DZ+\frac{k_Z}{{\omega_Z}^2}-\left(DZ+\frac{k_Z}{{\omega_Z}^2}\right)e^{-\alpha_Z t}\left(\frac{\alpha_Z\sin\sqrt{\omega_Z^2-\alpha_Z^2}\,t}{\sqrt{\omega_Z^2-\alpha_Z^2}}+\cos\sqrt{\omega_Z^2-\alpha_Z^2}\,t\right)$$

$$+ZNe^{-\alpha_Z t}\cos\sqrt{\omega_Z^2-\alpha_Z^2}\,t+\left(\alpha_Z ZN+ZVN\right)\frac{e^{-\alpha_Z t}}{\sqrt{\omega_Z^2-\alpha_Z^2}}\sin\sqrt{\omega_Z^2-\alpha_Z^2}\,t$$

$$Z_t=DZ+\frac{k_Z}{\omega_Z^2}+e^{-\alpha_Z t}\left(\left(ZN-DZ-\frac{k_Z}{\omega_Z^2}\right)\cos\sqrt{\omega_Z^2-\alpha_Z^2}\,t\right.$$

$$\left.+\frac{\left[\alpha_Z\left(ZN-DZ-\frac{k_Z}{\omega_Z^2}\right)+ZVN\right]\sin\sqrt{\omega_Z^2-\alpha_Z^2}\,t}{\sqrt{\omega_Z^2-\alpha_Z^2}}\right) \tag{6.21}$$

Introducing damping ratio, $\zeta=\frac{\alpha}{\omega}$, Equation 6.21 can be rewritten as:

$$Z_t=DZ+\frac{k_Z}{\omega_Z^2}+e^{-\zeta_Z\omega_Z t}\left(\left(ZN-DZ-\frac{k_Z}{\omega_Z^2}\right)\cos\omega_Z\sqrt{1-\zeta_Z^2}\,t\right.$$

$$+\frac{\left[\zeta_Z\omega_Z\left(ZN-DZ-\frac{k_Z}{\omega_Z^2}\right)+ZVN\right]\sin\omega_Z\sqrt{1-\zeta_Z^2}\,t}{\omega_Z\sqrt{1-\zeta_Z^2}}\Bigg) \tag{6.22}$$

Vertical velocity, *ZV*; acceleration, *ZA*; and jerk, *ZJ*, can be obtained by finding the first, second and third derivative of Equation 6.22 respectively.

$$ZV_t=\frac{dZ_t}{dt}=\left(ZN-DZ-\frac{k_Z}{\omega_Z^2}\right)\Bigg(-e^{-\zeta_Z\omega_Z t}\left(\omega_Z\sqrt{1-\zeta_Z^2}\cdot\sin\omega_Z\sqrt{1-\zeta_Z^2}\right)t$$

$$\zeta_Z\omega_Z\cos\omega_Z\sqrt{1-\zeta_Z^2}\,t\Big)\Big)+\frac{\zeta_Z\omega_Z\left(ZN-DZ-\frac{k_Z}{\omega_Z^2}\right)+ZVN}{\omega_Z\sqrt{1-\zeta_Z^2}}\cdot$$

$$\left(e^{-\zeta_Z\omega_Z t}\left(\omega_Z\sqrt{1-\zeta_Z^2}\cos\omega_Z\sqrt{1-\zeta_Z^2}\,t-\zeta_Z\omega_Z\sin\omega_Z\sqrt{1-\zeta_Z^2}\,t\right)\right)$$

$$=e^{-\zeta_Z\omega_Z t}\zeta_Z\omega_Z\left(\left(ZN-DZ-\frac{k_Z}{\omega_Z^2}\right)+\frac{ZVN}{\zeta_Z\omega_Z}-\left(ZN-DZ-\frac{k_Z}{\omega_Z^2}\right)\right)\cdot$$

$$\cos\omega_Z\sqrt{1-\zeta_Z^2}\,t-e^{-\zeta_Z\omega_Z t}\Bigg(\left(ZN-DZ-\frac{k_Z}{\omega_Z^2}\right)\left(\omega_Z\sqrt{1-\zeta_Z^2}\right)$$

$$+\frac{\zeta_Z^2\omega_Z^2\left(ZN-DZ-\frac{k_Z}{\omega_Z^2}\right)+\zeta_Z\omega_Z ZVN}{\omega_Z\sqrt{1-\zeta_Z^2}}\Bigg)\sin\omega_Z\sqrt{1-\zeta_Z^2}\,t$$

$$ZV_t=e^{-\zeta_Z\omega_Z t}\Bigg(ZVN\cos\omega_Z\sqrt{1-\zeta_Z^2}\,t$$

$$-\frac{\left[\omega_Z^2\left(ZN-DZ-\frac{k_Z}{\omega_Z^2}\right)+\zeta_Z\omega_Z ZVN\right]\sin\omega_Z\sqrt{1-\zeta_Z^2}\,t}{\omega_Z\sqrt{1-\zeta_Z^2}}\Bigg) \tag{6.23}$$

$$ZA_t=\frac{dZV_t}{dt}=e^{-\zeta_Z\omega_Z t}(ZVN)\left[-\omega_Z\sqrt{1-\zeta_Z^2}\,\sin\omega_Z\sqrt{1-\zeta_Z^2}\,t-\zeta_Z\omega_Z\,\cos\omega_Z\sqrt{1-\zeta_Z^2}\,t\right]$$

$$-e^{-\zeta_Z\omega_Z t}\left(\frac{\omega_Z^2\left(ZN-DZ-\frac{k_Z}{\omega_Z^2}\right)+\zeta_Z\omega_Z ZVN}{\omega_Z\sqrt{1-\zeta_Z^2}}\right).$$

$$\left[\left(\omega_Z\sqrt{1-\zeta_Z^2}\right)\cos\omega_Z\sqrt{1-\zeta_Z^2}\,t-\zeta_Z\omega_Z\sin\omega_Z\sqrt{1-\zeta_Z^2}\,t\right]$$

$$=e^{-\zeta_Z\omega_Z t}\left[\frac{\left(2\zeta_Z^2\omega_Z^2-\omega_Z^2\right)(ZVN)+\zeta_Z\omega_Z^3\left(ZN-DZ-\frac{k_Z}{\omega_Z^2}\right)}{\omega_Z\sqrt{1-\zeta_Z^2}}\sin\omega_Z\sqrt{1-\zeta_Z^2}\,t\right.$$

$$\left.-\left(2\zeta_Z\omega_Z ZVN+\omega_Z^2\left(ZN-DZ-\frac{k_Z}{\omega_Z^2}\right)\right)\cos\omega_Z\sqrt{1-\zeta_Z^2}\,t\right]$$

$$ZA_t=\omega_Z e^{-\zeta_Z\omega_Z t}\left[\frac{\left(2\zeta^2-1\right)(ZVN)+\zeta_Z\omega_Z\left(ZN-DZ-\frac{k_Z}{\omega_Z^2}\right)}{\sqrt{1-\zeta_Z^2}}\sin\omega_Z\sqrt{1-\zeta_Z^2}\,t\right.$$

$$\left.-\left(2\zeta_Z ZVN+\omega_Z\left(ZN-DZ-\frac{k_Z}{\omega_Z^2}\right)\right)\cos\omega_Z\sqrt{1-\zeta_Z^2}\,t\right] \tag{6.24}$$

$$ZJ_t = \frac{dZA_t}{dt} = \omega_Z \left\{ e^{-\zeta_Z \omega_Z t} \frac{(2\zeta^2 - 1)(ZVN) + \zeta_Z \omega_Z \left(ZN - DZ - \frac{k_Z}{\omega_Z^2} \right)}{\sqrt{1-\zeta_Z^2}} \cdot \right.$$

$$\left[\omega_Z \sqrt{1-\zeta_Z^2} \cos \omega_Z \sqrt{1-\zeta_Z^2}\, t - \zeta_Z \omega_Z \sin \omega_Z \sqrt{1-\zeta_Z^2}\, t \right]$$

$$- e^{\zeta_Z \omega_Z t} \left(2\zeta_Z ZVN + \omega_Z \left(ZN - DZ - \frac{k_Z}{\omega_Z^2} \right) \right) \cdot$$

$$\left. \left[-\omega_Z \sqrt{1-\zeta_Z^2} \sin \omega_Z \sqrt{1-\zeta_Z^2}\, t - \zeta_Z \omega_Z \cos \omega_Z \sqrt{1-\zeta_Z^2}\, t \right] \right\}$$

$$= \omega_Z e^{-\zeta_Z \omega_Z t} \left\{ \left[\omega_Z \left(4\zeta_Z^2 - 1 \right) ZVN + 2\zeta_Z \omega_Z^2 \left(ZN - DZ - \frac{k_Z}{\omega_Z^2} \right) \right] \cos \omega_Z \sqrt{1-\zeta_Z^2}\, t \right.$$

$$+ \frac{\omega_Z \left(2\zeta_Z - 2\zeta_Z^3 - 2\zeta_Z^3 + \zeta_Z \right) ZVN + \left(\omega_Z^2 - \zeta_Z^2 \omega_Z^2 - \zeta_Z^2 \omega_Z^2 \right) \left(ZN - DZ - \frac{k_Z}{\omega_Z^2} \right)}{\sqrt{1-\zeta_Z^2}}$$

$$\left. \sin \omega_Z \sqrt{1-\zeta_Z^2}\, t \right\}$$

$$ZJ_t = \omega_Z^2 e^{-\zeta_Z \omega_Z t} \left\{ \left[\left(4\zeta_Z^2 - 1 \right) ZVN + 2\zeta_Z \omega_Z^2 \left(ZN - DZ - \frac{k_Z}{\omega_Z^2} \right) \right] \cos \omega_Z \sqrt{1-\zeta_Z^2}\, t \right.$$

$$\left. + \frac{\left(3\zeta_Z - 4\zeta_Z^3 \right) ZVN + \left(\omega_Z - 2\zeta_Z^2 \omega_Z \right) \left(ZN - DZ - \frac{k_Z}{\omega_Z^2} \right)}{\sqrt{1-\zeta_Z^2}} \sin \omega_Z \sqrt{1-\zeta_Z^2}\, t \right\} \quad (6.25)$$

Consider a special case at $t = 0$, i.e. the vehicle is taking off. The state equations become:

$$Z_{t=0} = DZ + \frac{k_Z}{\omega_Z^2} + \left(ZN - DZ - \frac{k_Z}{\omega_Z^2} \right) = ZN \tag{6.26}$$

$$ZV_{t=0} = ZVN \tag{6.27}$$

$$ZA_{t=0} = -\omega_Z \left(2\zeta_Z ZVN + \omega_Z \left(ZN - DZ - \frac{k_Z}{\omega_Z^2} \right) \right) \tag{6.28}$$

$$ZJ_{t=0} = \omega_Z^2 \left[\left(4\zeta_Z^2 - 1 \right) ZVN + 2\zeta_Z \omega_Z^2 \left(ZN - DZ - \frac{k_Z}{\omega_Z^2} \right) \right] \tag{6.29}$$

6.3 Lateral Position Control

Considering lateral displacement, we allocate the desired lateral position at the centerline, i.e. $DY = 0$. The lateral component of wind gusting is the only force that causes the vehicle to sway off. Thus, analyzing by the same approach yields similar results of lateral displacement, velocity, acceleration, and jerk as follows:

$$Y(t) = \frac{k_Y}{\omega_Y^2} + e^{-\alpha_Y t} \left(\left(YN - \frac{k_Y}{\omega_Y^2} \right) \cos \omega_Y' t + \frac{\left[\alpha_Y \left(YN - \frac{k_Y}{\omega_Y^2} \right) + YVN \right] \sin \omega_Y' t}{\omega_Y'} \right) \tag{6.30}$$

$$YV(t) = e^{-\alpha_Y t} \left(YVN \cos \omega_Y' t - \frac{\left[\omega_Y^2 \left(YN - \frac{k_Y}{\omega_Y^2} \right) + \alpha_Y YVN \right] \sin \omega_Y' t}{\omega_Y'} \right) \tag{6.31}$$

$$YA(t) = \alpha_Y e^{-\alpha_Y t}\left(\frac{\left[\omega_Y^2 \left(YN - \frac{k_Y}{\omega_Y^2} \right) + \alpha_Y YVN \right] \sin \omega_Y' t}{\omega_Y'} - YVN \cos \omega_Y' t \right)$$

$$- \omega_Y' e^{-\alpha_Y t}\left(\frac{\left[\omega_Y^2 \left(YN - \frac{k_Y}{\omega_Y^2} \right) + \alpha_Y YVN \right] \cos \omega_Y' t}{\omega_Y'} - YVN \sin \omega_Y' t \right) \quad (6.32)$$

$$YJ(t) = e^{-\alpha_Y t}\left(2\alpha_Y^2 - \omega_Y^2\right) \cdot \left(YVN \cos \omega_Y' t - \frac{\left[\omega_Y^2 \left(YN - \frac{k_Y}{\omega_Y^2} \right) + \alpha_Y YVN \right] \sin \omega_Y' t}{\omega_Y'} \right)$$

$$+ 2\alpha_Y \omega_Y' e^{-\alpha_Y t}\left(YVN \sin \omega_Y' t + \frac{\left[\omega_Y^2 \left(YN - \frac{k_Y}{\omega_Y^2} \right) + \alpha_Y YVN \right] \cos \omega_Y' t}{\omega_Y'} \right) \quad (6.33)$$

where YN and YVN are the initial values of $Y(t)$ and $YV(t)$, $k_Y = \frac{WF_Y}{M}$, and $\omega_Y' = \sqrt{\omega_Y^2 - \alpha_Y^2}$

The magnetic and damping forces vertically and laterally attract and stabilize the vehicle back to its desired position. The magnitudes of these two forces are major concerns since they affect accelerations and jerks. The maximum acceleration and jerk allowed in any axis are 32.2 ft/sec^2 and 16.1 ft/sec^2 respectively. Weak magnetic force fails to control the vehicle within its allowable displacement, while too strong magnetic force results in sudden changes of acceleration. Likewise, weak damping force cannot prevent the vehicle from excess oscillation, while too strong damping force increases jerk of the vehicle.

6.4 Lateral Position Control on Horizontal Curve

When a vehicle from a straight-line motion entering a curved path, changes in its direction generate centrifugal acceleration, and thus force as a function of square of speed. The banking of the roadway cross section, referred to as superelevation, is utilized to balanced the centripetal force with the vehicle's own weight. For a conventional tire-on pavement, the maximum superelevation rate should not exceed 0.10 [80] which accommodates a vehicle entering a 1,500-ft radius curve at maximum speed of 80 mph. To integrate guideway facility to the existing freeway, the 1,500-ft radius is taken as an extreme value in designing the control law.

Consider a free-body diagram of a maglev vehicle entering a curve with a superelevation rate q as shown in Fig. 6.1, five major forces acting on the maglev vehicle are centrifugal force c, lateral magnetic force F_y, vertical magnetic force F_x, the vehicle's weight w, and lift force L. Assuming that while traveling along the curve path the vehicle is at a constant speed that balances its weight with the lift force and the vertical magnetic propulsion force, the equilibrium of the forces can be expressed as

$$c\cos\theta = F_y$$

$$\frac{v^2}{r}\cos\theta = \quad YK \times Y - YD \quad YV \tag{6.34}$$

where is the vehicle speed, r Y is lateral position, is a suspension magnetic constant, is lateral speed, and YD

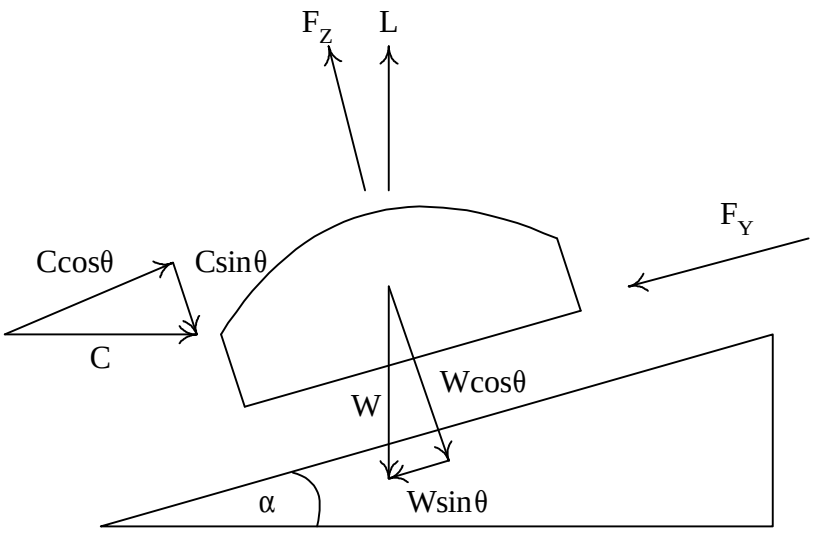

Figure 6.1 Free body diagram of a maglev vehicle on a curvature path

However, the two forces in equation (6.34) may not be balance at all time. This would cause the vehicle to sway out of the desired position. We take differential equations of position and speed of the vehicles to find the expression of *Y* and *YV* as a function of time.

$$\frac{dY_t}{dt} = YC_t \tag{6.35}$$

$$\frac{dYV_t}{dt} = YAC_t - YAP_t - YAD_t$$

$$= \frac{v^2}{r}\cos\theta - \frac{YK}{M} \times Y - \frac{YD}{M} \times YV \tag{6.36}$$

where YC_t = rate of change of lateral position at time *t*

YAC_t = lateral acceleration due to centrifugal force at time *t*

YAP_t = lateral acceleration due to magnetic propulsion at time *t*

YAD_t = lateral acceleration due to damping at time *t*

Following the same steps in solving differential equations, we get the expression of lateral position $Y(t)$, speed $YV(t)$, acceleration $YA(t)$, and jerk $YJ(t)$ as:

$$Y(t) = \frac{v^2}{r}\cdot\frac{\cos\theta}{\omega_Y^2} + e^{-\alpha_Y t}\left(YN - \frac{v^2}{r}\cdot\frac{\cos\theta}{\omega_Y^2}\right)\cos\omega_Y\sqrt{1-\zeta_Y^2}\,t + \frac{e^{-\alpha_Y t}\left[\alpha\left(YN - \frac{v^2}{r}\cdot\frac{\cos\theta}{\omega_Y^2}\right) + YVN\right]\sin\omega_Y\sqrt{1-\zeta_Y^2}\,t}{\omega_Y\sqrt{1-\zeta_Y^2}} \tag{6.37}$$

$$YV(t) = e^{-\alpha_Y t}\left(YVN\cos\omega_Y\sqrt{1-\zeta_Y^2}\,t - \frac{\left[\omega_Y\left(YN - \frac{v^2}{r}\cdot\frac{\cos\theta}{\omega_Y^2}\right) + \alpha_Y YVN\right]\sin\omega_Y\sqrt{1-\zeta_Y^2}\,t}{\omega_Y\sqrt{1-\zeta_Y^2}}\right) \tag{6.38}$$

$$YA(t) = \alpha_Y e^{-\alpha_Y t}\left(\frac{\left[\omega_Y^2\left(YN - \frac{v^2}{r}\cdot\frac{\cos\theta}{\omega_Y^2}\right) + \alpha_Y YVN\right]\sin\omega_Y\sqrt{1-\zeta_Y^2}\,t}{\omega_Y\sqrt{1-\zeta_Y^2}}t - YVN\cos\omega_Y\sqrt{1-\zeta_Y^2}\,t\right) - e^{-\alpha_Y t}\omega_Y\sqrt{1-\zeta_Y^2}\left(\frac{\left[\omega_Y^2\left(YN - \frac{v^2}{r}\cdot\frac{\cos\theta}{\omega_Y^2}\right) + \alpha_Y YVN\right]\cos\omega_Y\sqrt{1-\zeta_Y^2}\,t}{\omega_Y\sqrt{1-\zeta_Y^2}}\right.$$

$$+ YVN \sin \omega_Y \sqrt{1-\zeta_Y^2}\, t \Bigg) \tag{6.39}$$

Since a maglev vehicle is operated at very high speed but in as small radius as those of existing freeways, it is predictable that the lateral magnetic force has to be strong. The increase in F_y alone will result in high acceleration and jerk. Thus, in order to cancel the centripetal force while maintaining acceptable level of ride comfort, high superelevation rate is required. The transition spiral curve is introduced between the tangent section and the circular path to smoothen the development of superelevation. Practically, in high speed rail, a cubic parabolic curve is usually applied instead of theoretical clothoid curve for simplicity in construction.

In high speed rail industry, not only does the rail is superelevated, but the vehicle is also tilted to a desired angle. The objective of tilting the vehicle is to achieve an acceptable ride quality without investing large sums of money on very large radius track [81]. This concept can be as well applied to the maglev operation. Operating at higher speeds than conventional high speed rails, the maglev vehicle's tilted angles will be steeper. The expected value of aggregate banking ranges between 30 to 40 degrees. To achieve such high banking while keeping acceleration and jerk at an acceptable level, it is necessary that the vehicle starts to tilt on the tangent section. In doing so, the vehicle compartment rotation will gradually developed before entering the transition curve. Then it will continue rotating in the transition section until the combined magnitude of tilting and superelevation reach a desired angle right before entering the curvature path. Similarly, the inverse process is developed when the vehicle leaves the circular and transition curve to the tangent section.

Although the superelevation and tilt technology provide the means of high speed maglev operation in horizontal curve, it is expected that the speed in the circular path will still have to be reduced. Since the guideway design is based on separated operations for cars and trucks, the design speed and the tilted angle for each type will be individually considered according to sizes and weight of the vehicles.

6.5 Longitudinal Control

As stated in Chapter 5, maglev vehicles should be governed by different control schemes based on several thresholds of headways, speeds, and accelerations realized. In this preliminary step, a three-phase control rule is applied to determine the longitudinal position of the vehicles: viz.

$$\ddot{x}_i(t) = \begin{cases} -c^2 k_{i-j,i+p}(t-T)\left(\partial k / \partial x\right)_{i-j,i+p}(t-T), & x_{i-1} - x_i \geq S_p \\ b\left[x_{i-1}(t-T) - x_i(t-T) - S_c\right]^l, & S_p \geq x_{i-1} - x_i \geq S_c \\ XAP(t) - XAD(t), & x_{i-1} - x_i \leq S_c \end{cases} \tag{6.40}$$

where the notations are the same as noted in Section 2.6.1.

The physical meaning of equation (6.40) can be explained that a vehicle reacts to state changes of the leading vehicle differently depending on the spacing between the two. Two spacing thresholds, which are assumed constant, control the switching between modes. Spacing S_p refers to maximum acceptable spacing between vehicles that are considered platooned, and S_c refers to maximum allowable spacing between vehicles that are still under each other's magnetic influence. While the following vehicle is not platooned with the leading vehicle (i.e. spacing is more than S_p), it will response according to a macroscopic car-following law to decrease the spacing. When the spacing is closer and falls between S_p and S_c, the vehicle is controlled by spacing dependent function to adjust its headway closer to the leading vehicle. Eventually, when the following vehicle approaches the leading vehicle closely enough to be under each other's magnetic control, the rule of magnetism is applied.

A closed-form solution of 6.40 cannot be simply determined since each mode involves states of two or more vehicles. Computer simulation part of system dynamics is brought in to find a stepwise solution. Taking a platoon of four vehicles as an example scenario, the causal diagram is illustrated in figure 6.2.

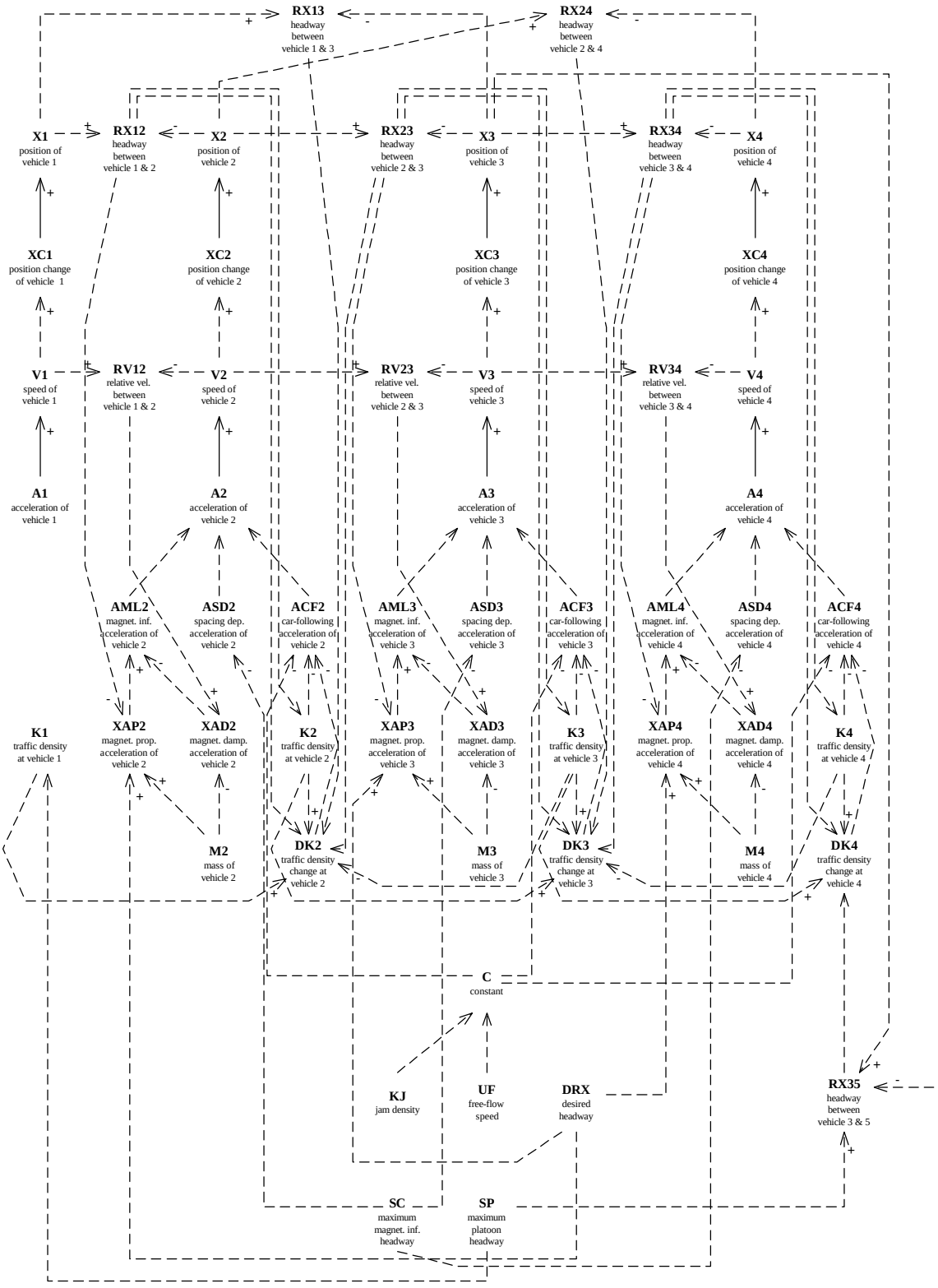

Figure 6.2 Causal diagram for four vehicles under the 3-phase control rule

6.6 Three-Dimensional Control Model

A three-dimensional control model is constructed to simulate a single vehicle traveling along a straight section of a guideway. These displacements are controlled by three Maglev technology functions — suspension, guidance and propulsion. In each dimension, there is a magnetic force to restore position and a magnetic damping force to reduce oscillations. The external forces acting on the vehicle involve lift force and wind forces on lateral and vertical axis as mathematically derived in Section 6.2 and 6.3.

Parameter selection necessarily involves magnetic and damping constants on all three axes. These constants contribute to magnetic forces, velocities, accelerations and jerks. Magnetic constants cannot be too small otherwise it will fail to restore the vehicle position once the vehicle sways off. Yet, large values of magnetic constants result in sudden changes of acceleration and excessive jerks. To achieve ride comfort, the maximum acceleration and jerk allowed in any axis should not exceed 32.2 ft/sec^2 and 16.1 ft/sec^2 respectively.

Among three kinds of oscillation motion, a critical damping is the most desirable since it provides stability for ride comfort. In order to achieve such a condition, the damping constant is necessarily fixed as

$$D = \sqrt{4 \times K \times M} \tag{6.41}$$

where K is magnetic constant and M is vehicle mass.

The results of the simulation are shown in Fig 6.3 for values XK = 500, YK = 15 and ZK = 15 lbs/ft for magnetic constants on X-, Y- and Z-axes respectively. In fact, the magnetic constant on all axes can vary over a wide allowable range that would not cause excessive accelerations and jerks. An exception is made that the magnetic constant on X-axis must be large since it is the axis with high-speed and high-acceleration movements. One should realize that the model depicts a simple scenario of straight section operation with almost identical traffic characteristics of each vehicle. The allowable ranges of

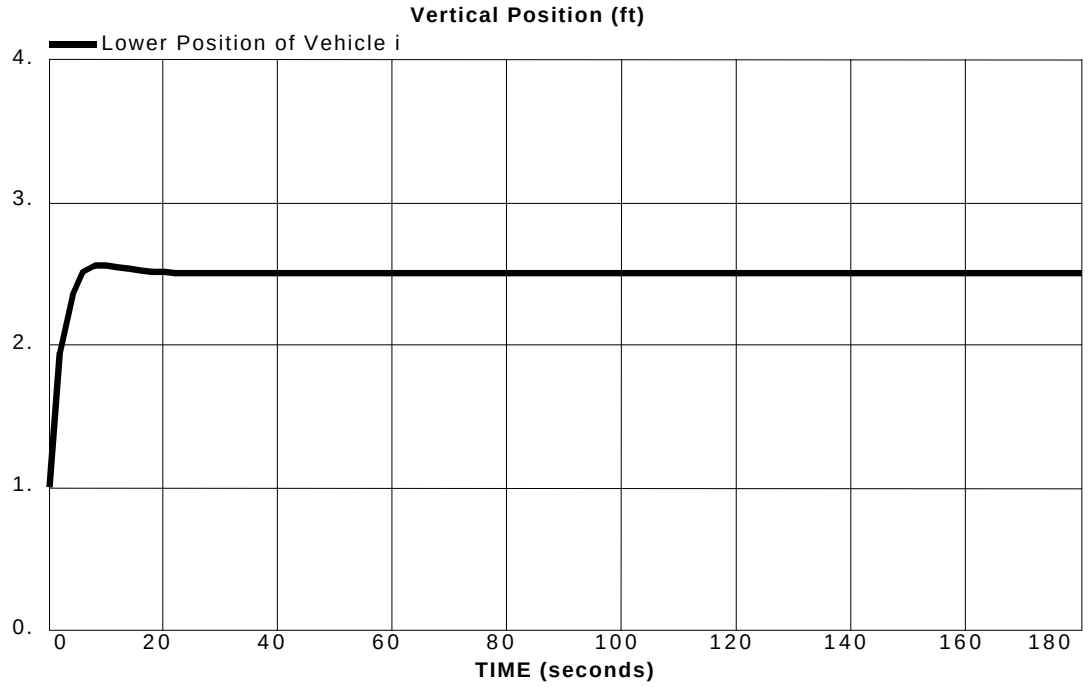

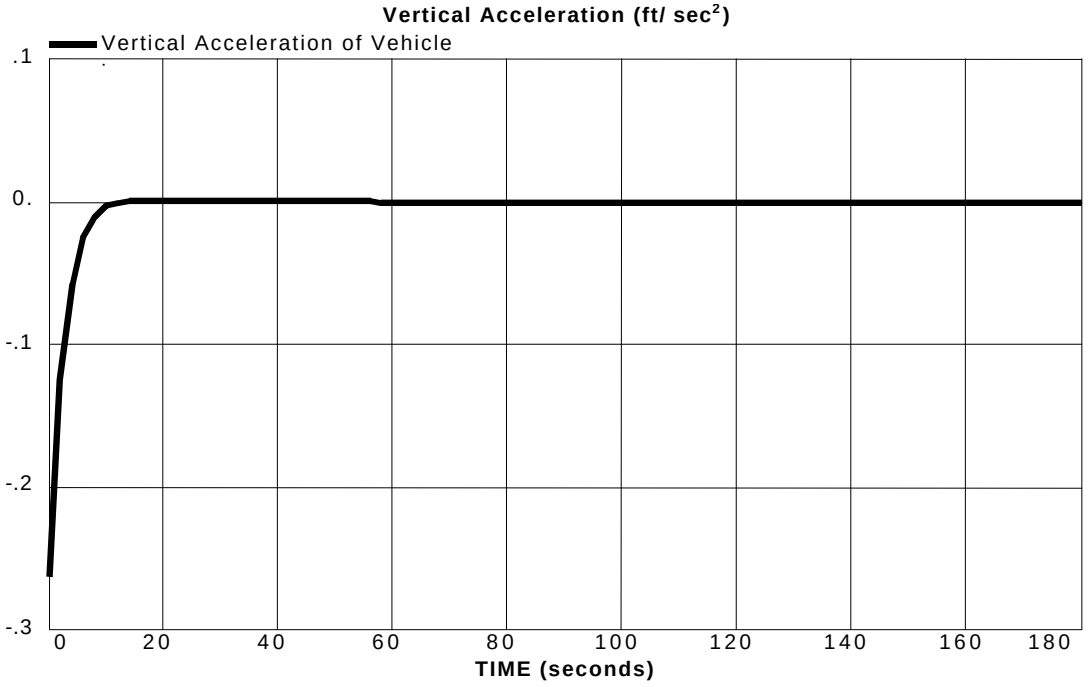

Figure 6.3 Vehicle Charcteristics under Three Dimensional Control Law

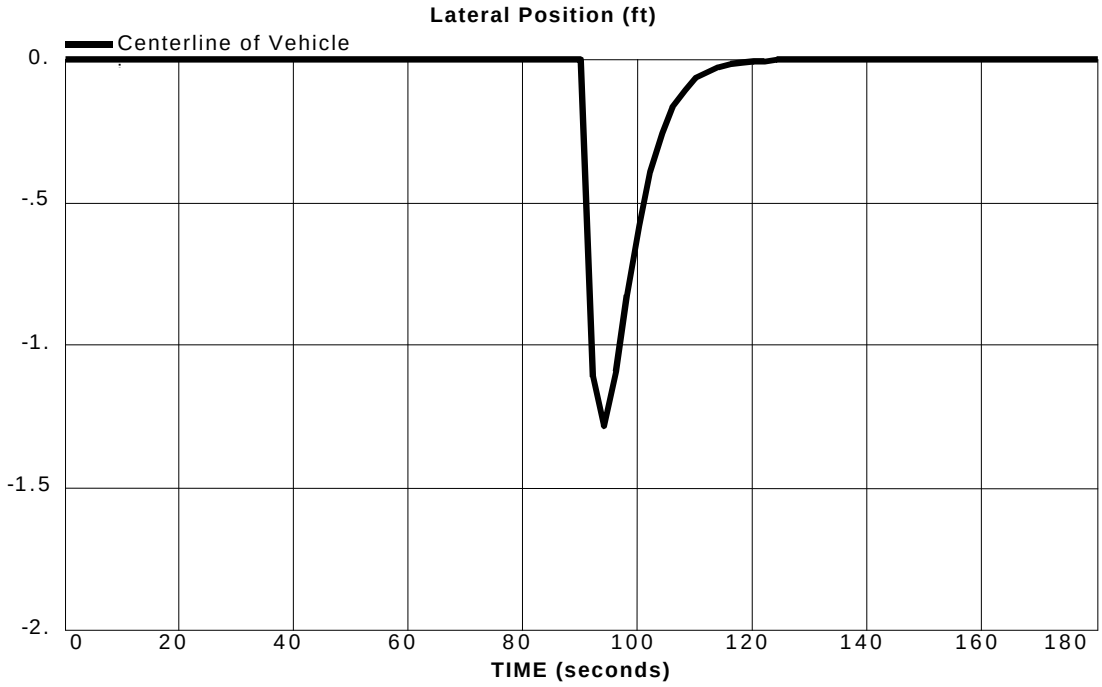

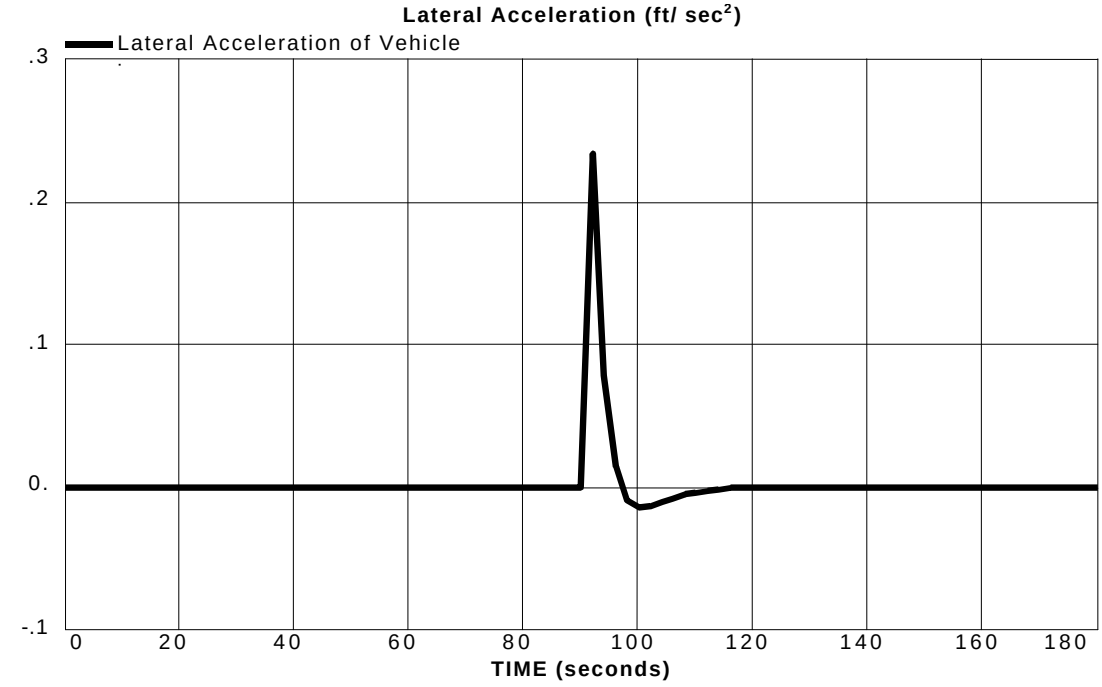

Figure 6.3 (cont'd) Vehicle Charcteristics under Three Dimensional Control Law

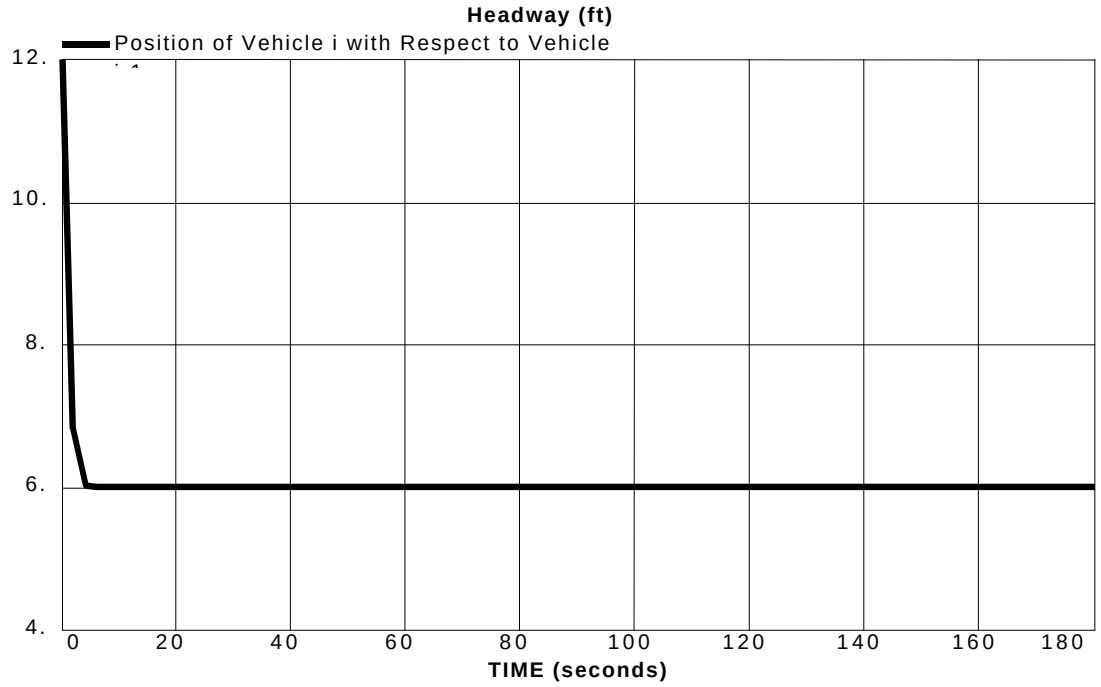

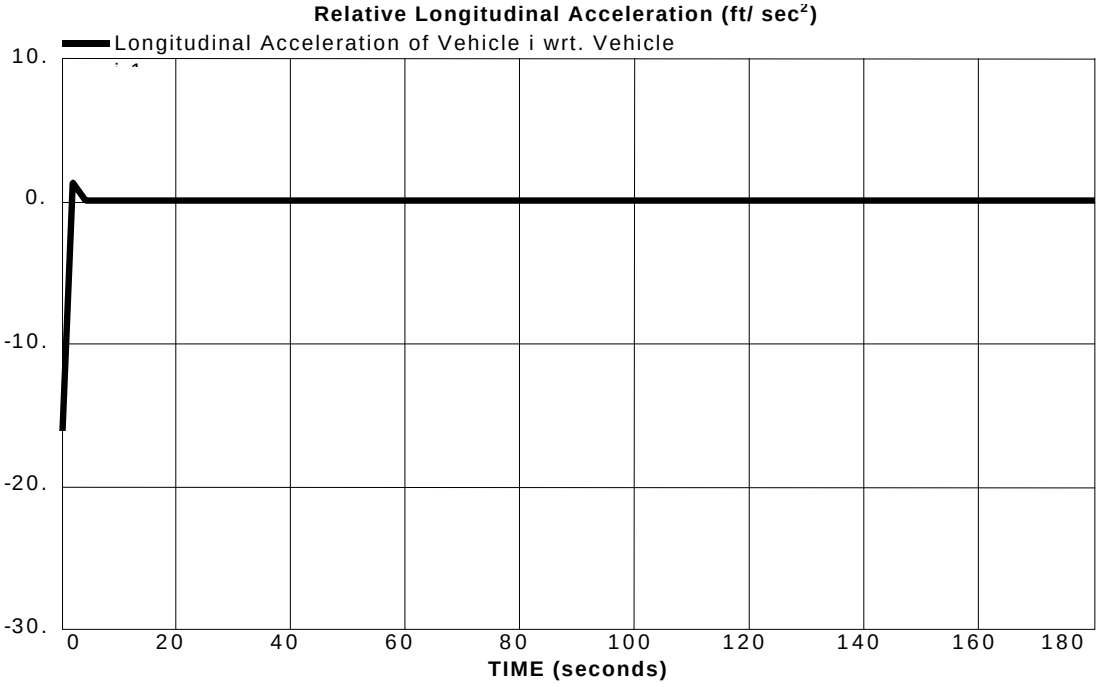

Figure 6.3 (cont'd) Vehicle Charcteristics under Three Dimensional Control Law

magnetic constants should be narrowed down when complicated conditions are applied, which will be further explored in following sections.

6.7 Longitudinal Control Models

Three longitudinal control laws including car maneuvering, spacing dependent and magnetic coupling, have been simulated. The models consist of a platoon of four vehicles which have initial velocity of 150 mph. The leading vehicle starts accelerating at time t = 0 with a rate of 0.2g until it reaches a cruising speed of 400 mph. Then at time t = 180 seconds, it decelerates at –0.2g until it comes to a complete stop. The following vehicles react to the changes of each predecessor under each govern rule. Their trajectories, velocities, and accelerations are investigated. Desired conditions are to keep close spaces between vehicles while avoiding collisions, intense accelerations, and excessive changes in accelerations.

6.7.1 Car Maneuvering Control Model

Vehicles in traffic stream are treated as if they are fluid particles [69]. A vehicle moves in one direction, as its response to the prevailing condition is highly susceptible in a high concentration area, and slow in a low concentration area. It gains acceleration when it moves from high to low concentrations, i.e. spacing between the vehicle and its successor is higher than that between the vehicle and its predecessor. On the reverse situation, the vehicle tends to decelerate. Unlike fluid particles, this feedback process takes some short period of time T to react to the prevailing condition. The equation for fluid analogous car maneuvering is expressed as follows:

$$\ddot{x}(t) = -c^2 k_{i-j,i+p}(t-T)\left(\partial k / \partial x\right)_{i-j,i+p}(t-T) \tag{6.42}$$

where the notations are the same as given in Section 5.5. Consider the special case where j = 1 and p = 0 we have the usual car-following formulation, which is applied to the simulation.

Changes of density k with respect to position x have to be estimated by Lagrange transformation. The transformation requires at least three data points. Thus, two imagery vehicles has to be modeled – one leading the first vehicle and another following the fourth vehicle – to create headway values for the first and the fifth vehicles. The two imagery vehicles are assumed to be in separated platoon, thus keep a constant headway of S_p at all time.

Constant C can be evaluated from fluid's equation of continuity as follows:

$$\frac{\partial k}{\partial t} + \frac{\partial q}{\partial x} = 0$$

Since $q = ku$,

$$\frac{\partial k}{\partial t} + \frac{\partial (ku)}{\partial x} = 0$$

$$\frac{\partial k}{\partial t} + \frac{u\partial k}{\partial x} + \frac{k\partial u}{\partial x} = 0 \qquad (6.43)$$

where $u = f(k)$,

Thus, $\frac{\partial u}{\partial k} = \frac{\partial u}{\partial x} \cdot \frac{\partial x}{\partial k} = \frac{du}{dk} = u'$

and $$\frac{\partial u}{\partial x} = u' \frac{\partial k}{\partial x} \qquad (6.44)$$

Substituting (6.44) into (6.43)

$$\frac{\partial k}{\partial t} + (u + u'k) \frac{\partial k}{\partial x} = 0 \qquad (6.45)$$

From $\frac{\partial u}{\partial t} = -c^2 k \frac{\partial k}{\partial x}$

$$\frac{\partial u}{\partial x}\cdot\frac{dx}{dt}+\frac{\partial u}{\partial t}\cdot\frac{dt}{dt}=-c^2k\frac{\partial k}{\partial x}$$

$$u\frac{\partial u}{\partial x}+\frac{\partial u}{\partial t}=-c^2k\frac{\partial k}{\partial x} \tag{6.46}$$

Since $\frac{\partial u}{\partial t}=\frac{du}{dk}\cdot\frac{\partial k}{\partial t}=u'\frac{\partial k}{\partial t}$

Equation (6.46) is equivalent to

$$\frac{\partial k}{\partial t}+\left(u+\frac{c^2k}{u'}\right)\frac{\partial k}{\partial x}=0 \tag{6.47}$$

Comparing (6.45) and (6.47), we get

$$(u')^2=c^2$$

From the inverse relationship between speed and density, it can be seen that

$$\frac{du}{dk}=-c$$

By integrating from 0 to free flow speed u_f and from jam density k_j to zero density, we get

$$\int_0^{u_f}du=-\int_{k_j}^{0}cdk$$

$$u_f=ck_j$$

$$c=\frac{u_f}{k_j} \tag{6.48}$$

The problem is still being raised on definitions of “free flow speed” and particularly “jam density”. As previous assumed, Maglev vehicles should reach a top speed of 450 mph, thus this value is allocated to u_f. Jam density is parameter that is difficult to estimate since there will scarcely exist such “jam condition” in Maglev

operation. An alternative is to estimate an average space occupied by a stop maglev vehicle plus some spacing on its front and back. By doing so, k_j is estimated to be 1 vehicle per 8 feet or 660 vehicles per mile.

By evaluating constant C, the problem leaves out only the selection of reaction time *T*. We explore the effect of reaction time T to headways, velocities, and accelerations by mean of sensitivity analysis as the results are shown in Figure 6.4. As one might expect, long reaction times create high fluctuations on vehicle velocities and accelerations, while a short 0.05 seconds reaction time reduces some oscillations.

Nonetheless, regardless of how small reaction time is, car maneuvering law falls short to reduce asymptotic instability since the vehicles are operated at very high speed. By the time a following vehicle detects and reacts to speed and acceleration changes of a leading vehicle, it fails to properly adjust its acceleration safely and comfortably. The vehicle are accelerating and decelerating to the maximum allowing values within short periods of time. These switches cause excessive jerks, which can be injurious for the riders. Even so, since the maximum acceleration/deceleration rate is set to ± 32 ft/sec^2 or 1g, the vehicles cannot decelerate fast enough after detecting its predecessor's slowing down or stop, and eventually come to collisions after a short period.

6.7.2 Spacing Dependent Control Model

Traditional car following models (i.e., GM's model and car maneuvering model) fail to explain the response of vehicles with identical speeds. Spacing dependent model is rectified based on spacing to eliminate such deficiency of traditional models. Consider the following spacing dependent model:

$$\ddot{x}(t) = b\left[x_{i-1}(t-T) - x_i(t-T) - S_c\right]^l \qquad (6.49)$$

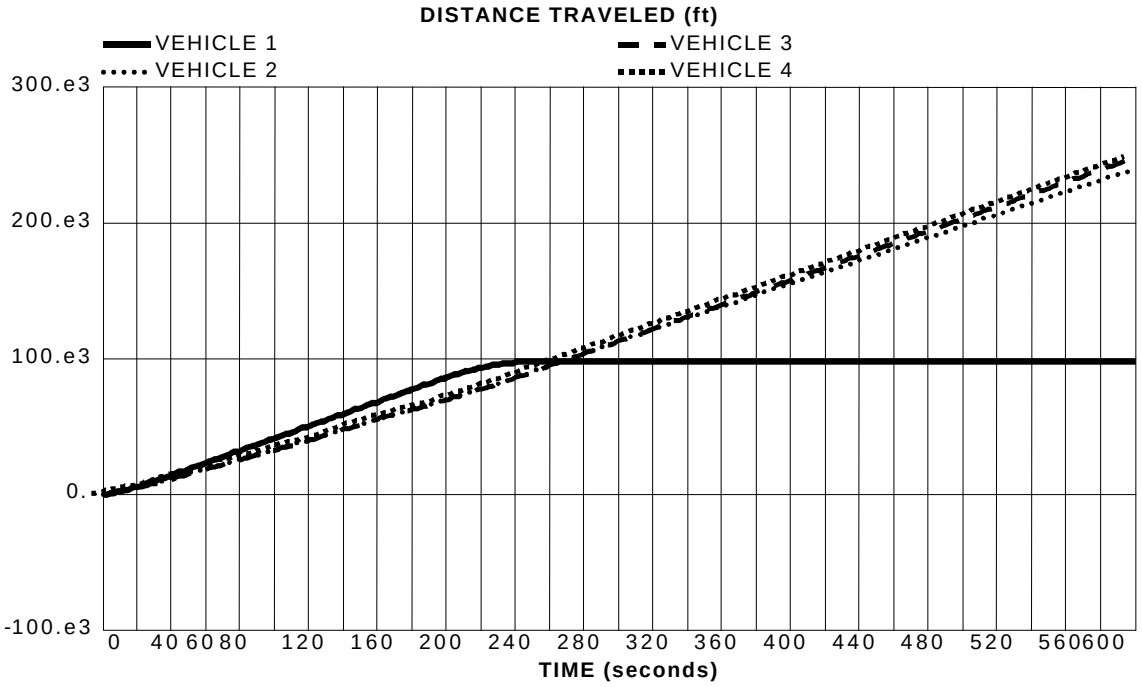

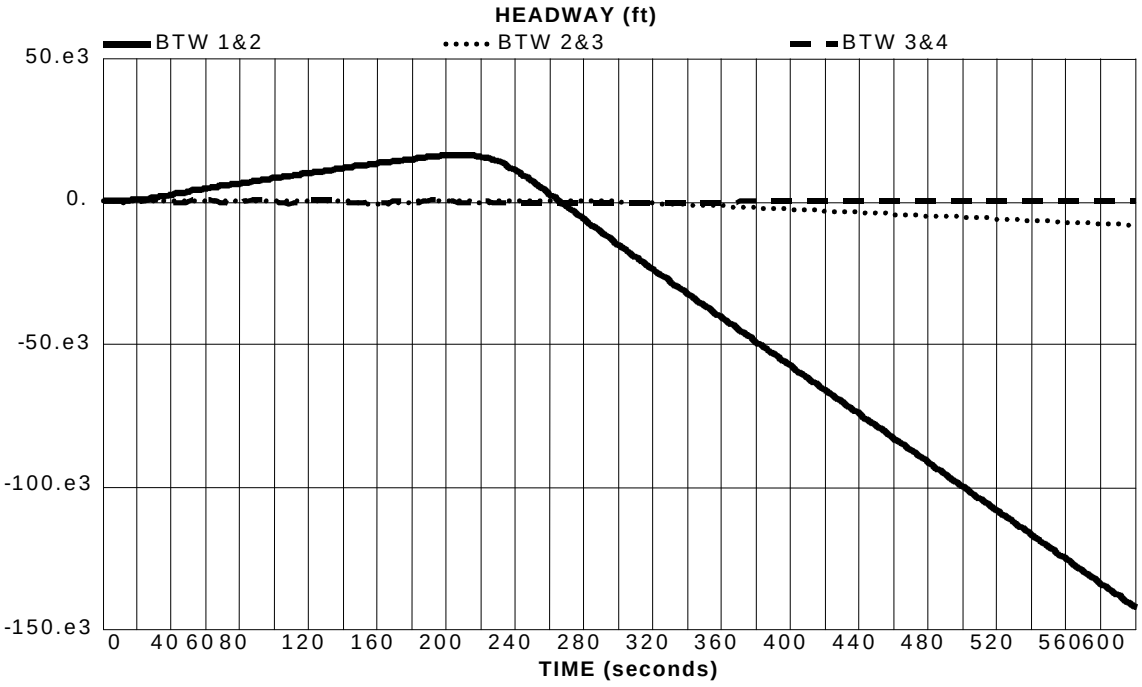

Figure 6.4a Vehicle Characteristics under Car Maneuvering Model (T = 0.2 seconds)

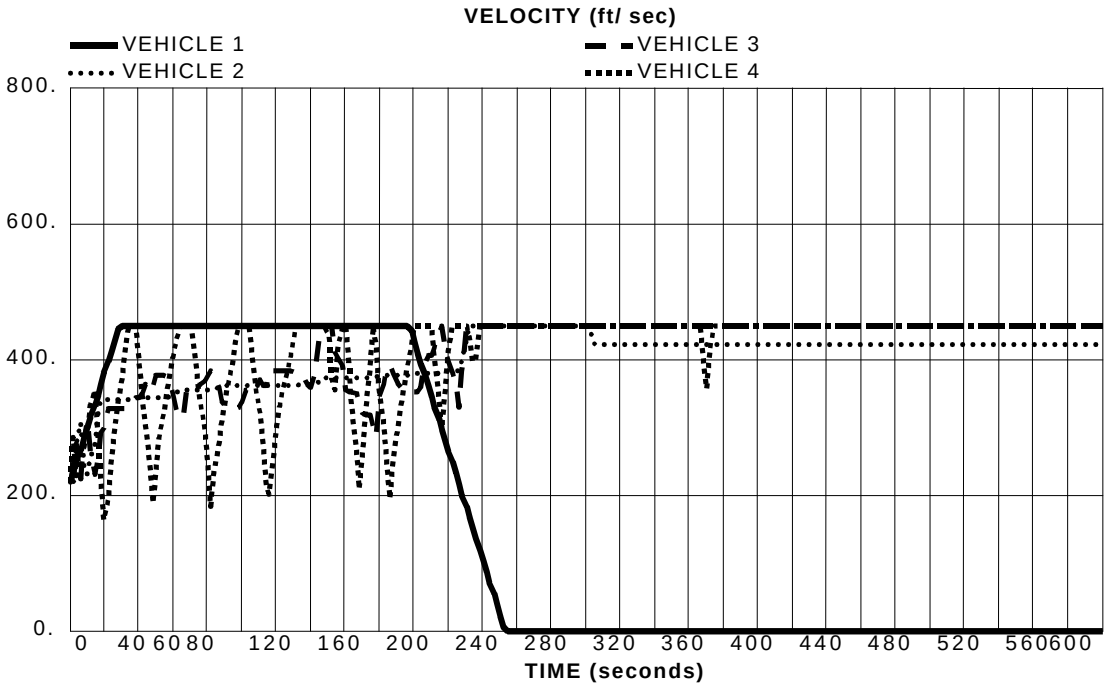

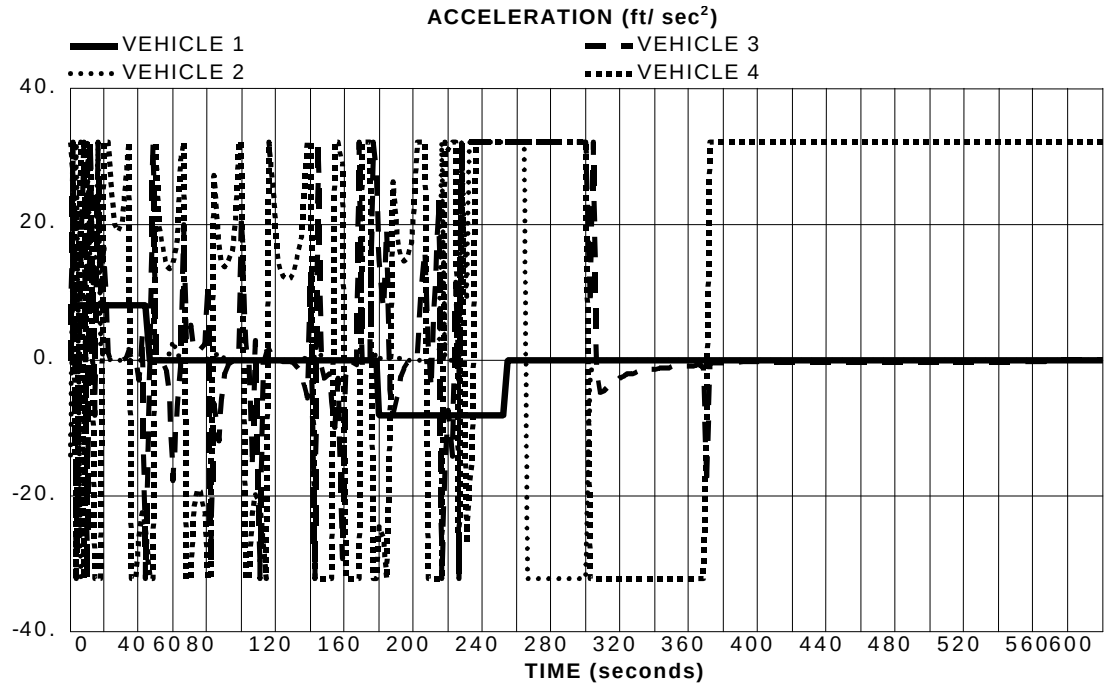

Figure 6.4a (cont'd) Vehicle Characteristics under Car Maneuvering Model (T = 0.2 seconds)

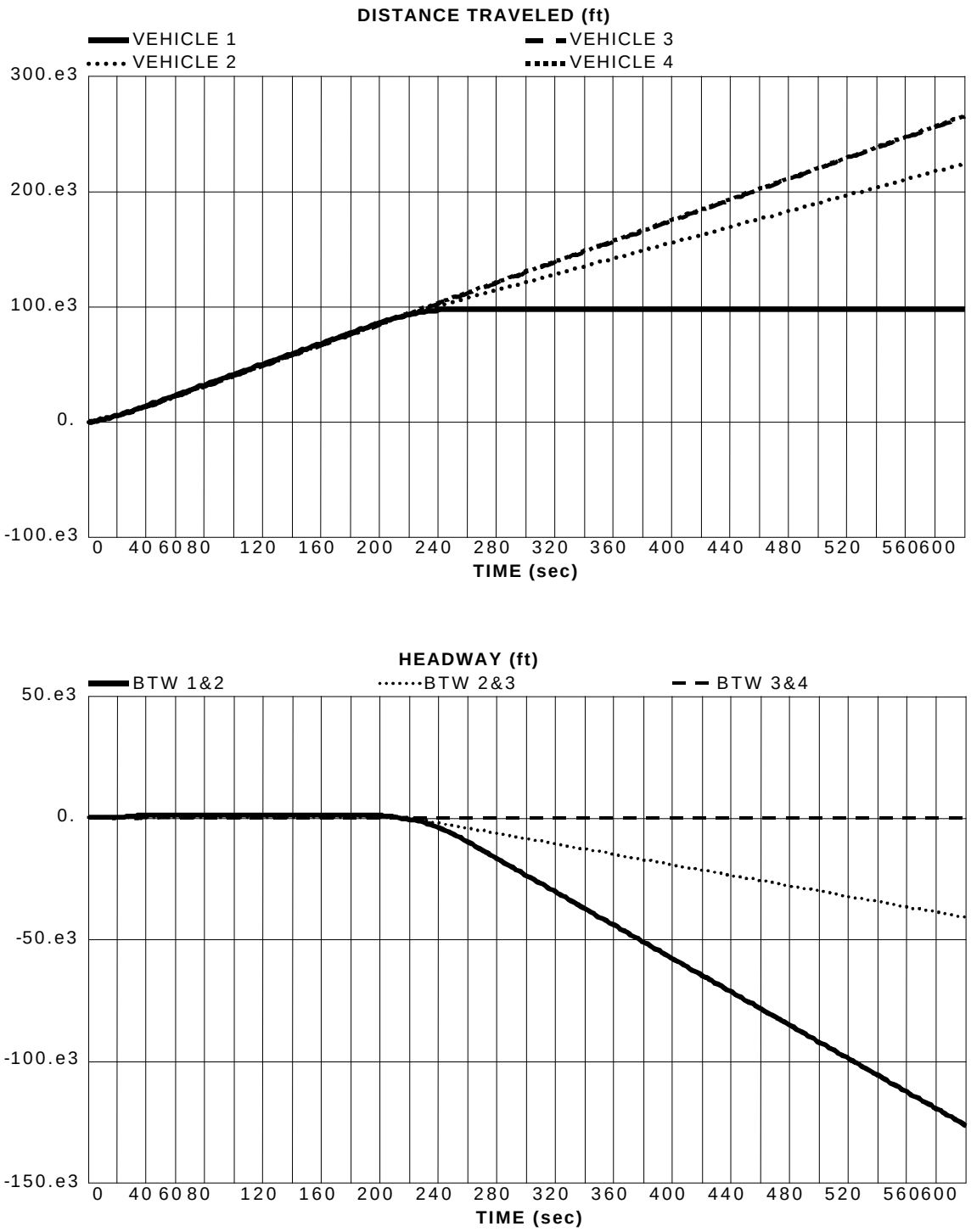

Figure 6.4b Vehicle Characteristics under Car Maneuvering Model (T = 0.1 seconds)

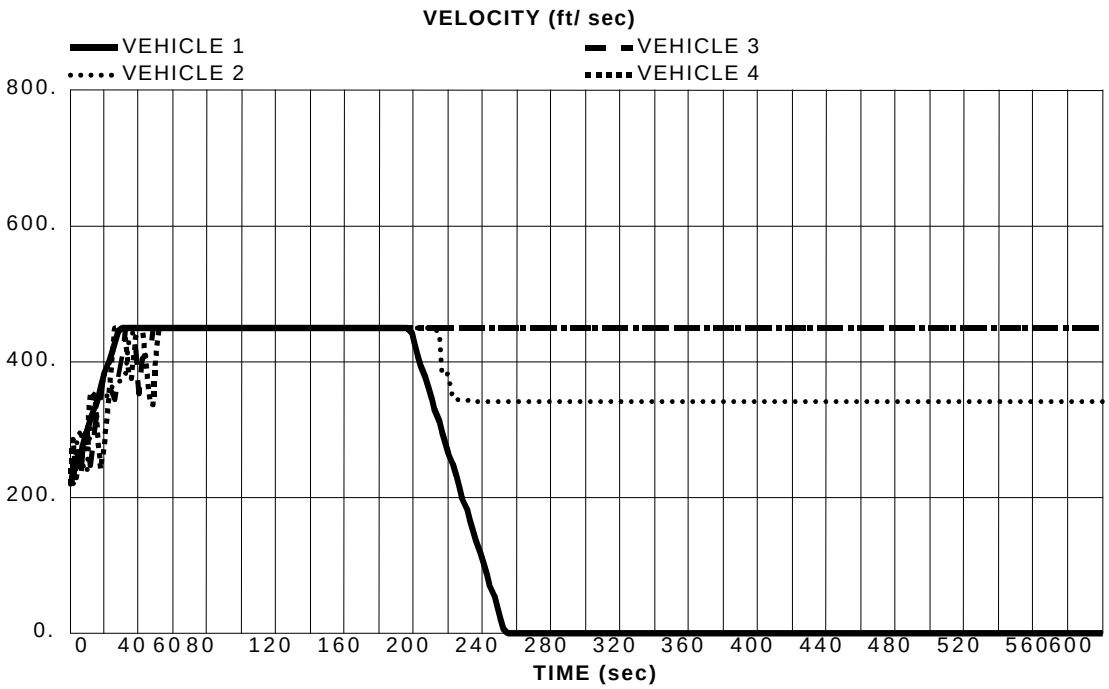

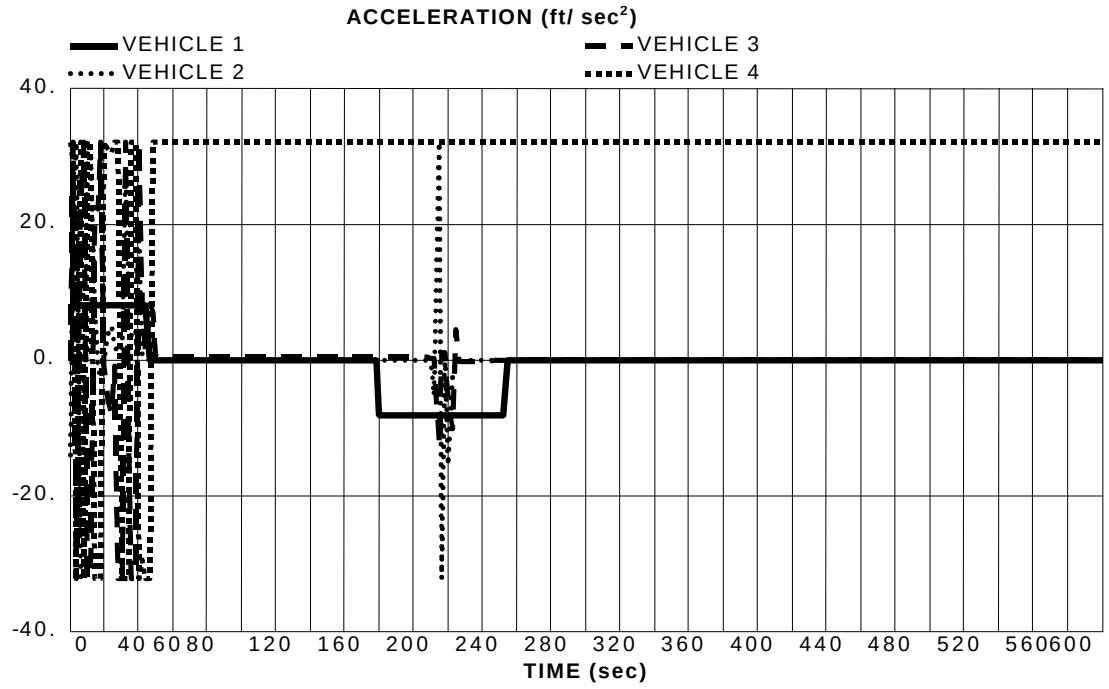

Figure 6.4b (cont'd)Vehicle Characteristics under Car Maneuvering Model (T = 0.1 seconds)

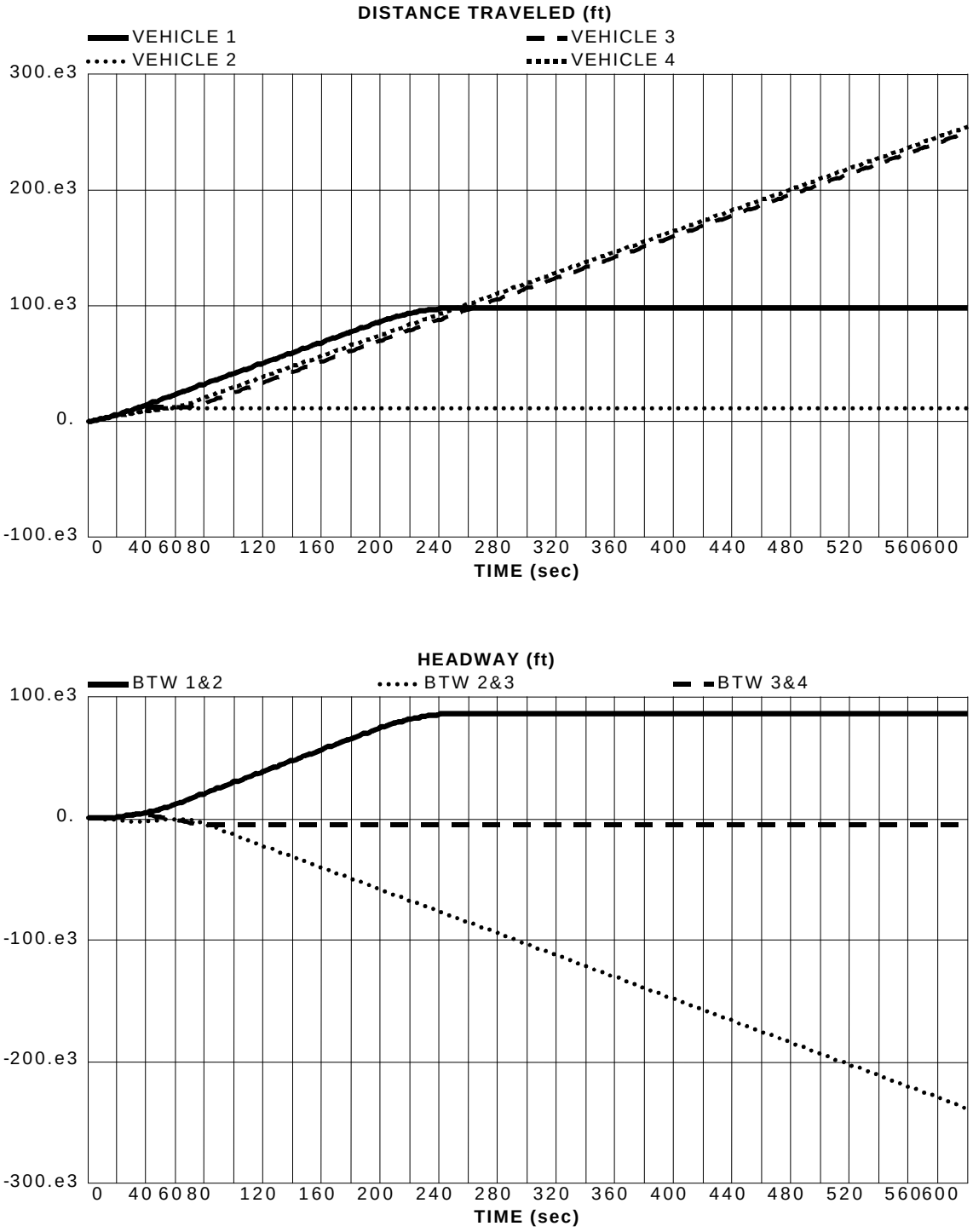

Figure 6.4c Vehicle Characteristics under Car Maneuvering Model (T = 0.05 seconds)

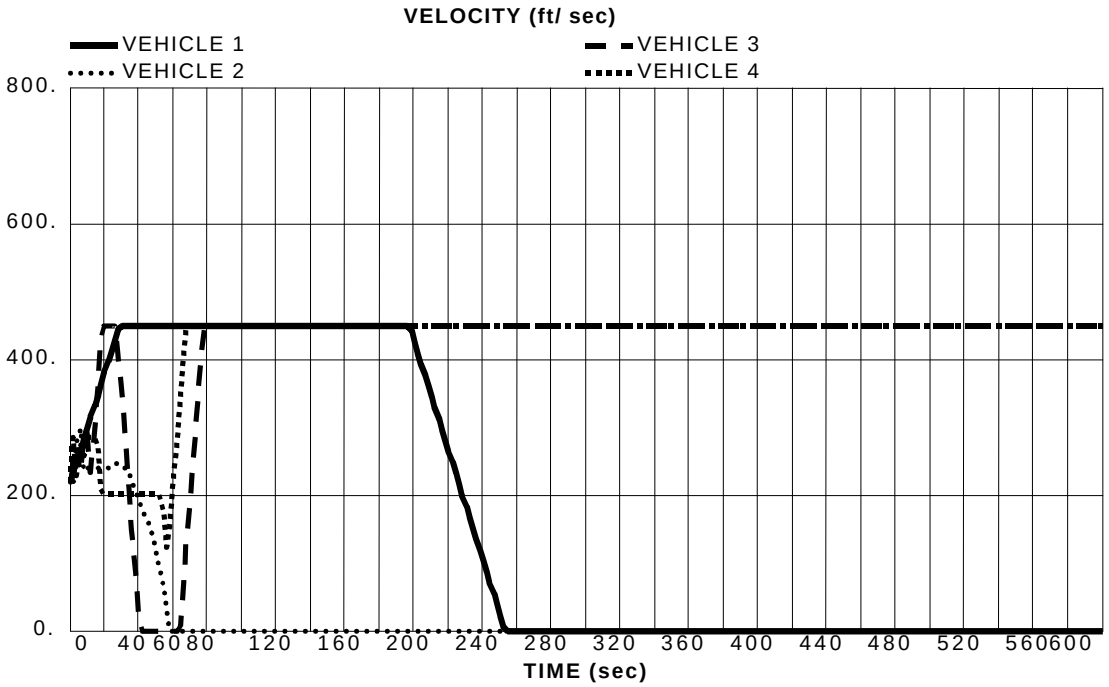

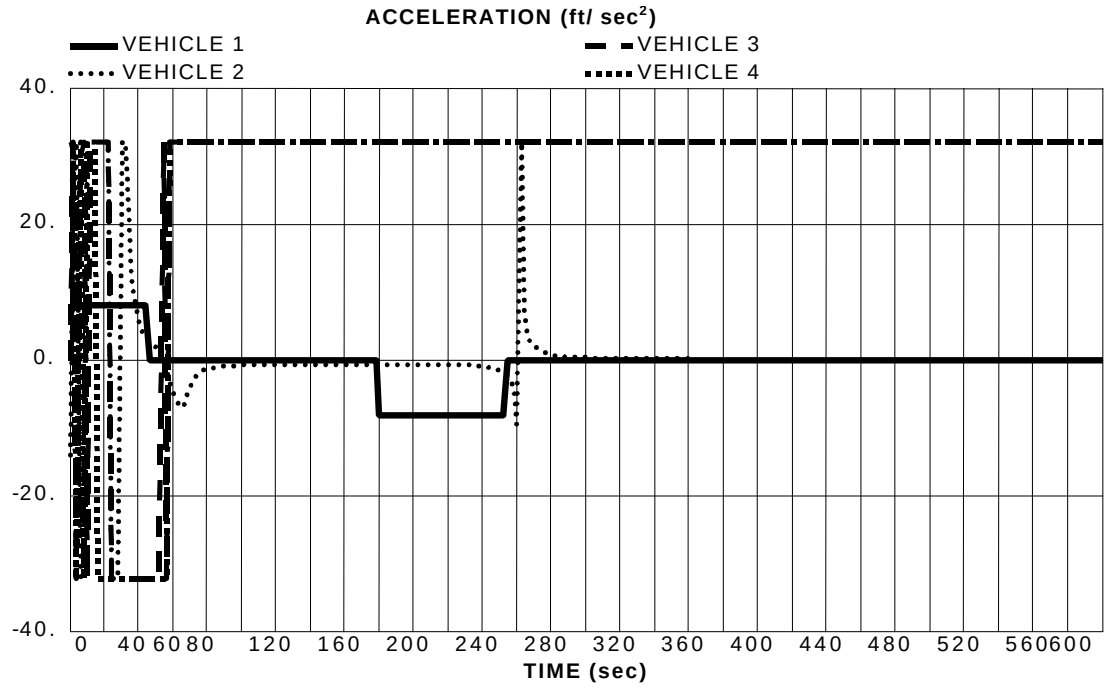

Figure 6.4c (cont'd)Vehicle Characteristics under Car Maneuvering Model (T = 0.05 seconds)

Two parameters required to be explored here are constants *b* and *l*. Parameter *l* is constraints to odd integers in order to allow the equation to segregate accelerations from decelerations. For sake of simplicity, *l* is fixed as 3, which is the lowest nonlinear power to keep the equation in the desired condition. Range of *b* is being tested from 0.01 to 0.0001. The results of sensitivity analysis are shown in Fig 6.5.

The value *b* does not show significant effects on pattern of velocities and accelerations. The use of small values of *b* improves the chance of a vehicle to stop. The second vehicle almost avoid the collision with the first vehicle when as small *b* as 0.0001 is used.

The results show very strong fluctuations of velocities and accelerations when vehicles start to adjust themselves to stable condition. Had it not been bounded by maximum ± 32 ft/sec^2 constraints, the fluctuation could have created as high jerk as 180 ft/sec^2. As the operation proceeds, remarkably smooth adjustments of these values can be noticed. The same problem raises when the leading vehicle stop, the high speed of the following vehicle is carried over and causes collision.

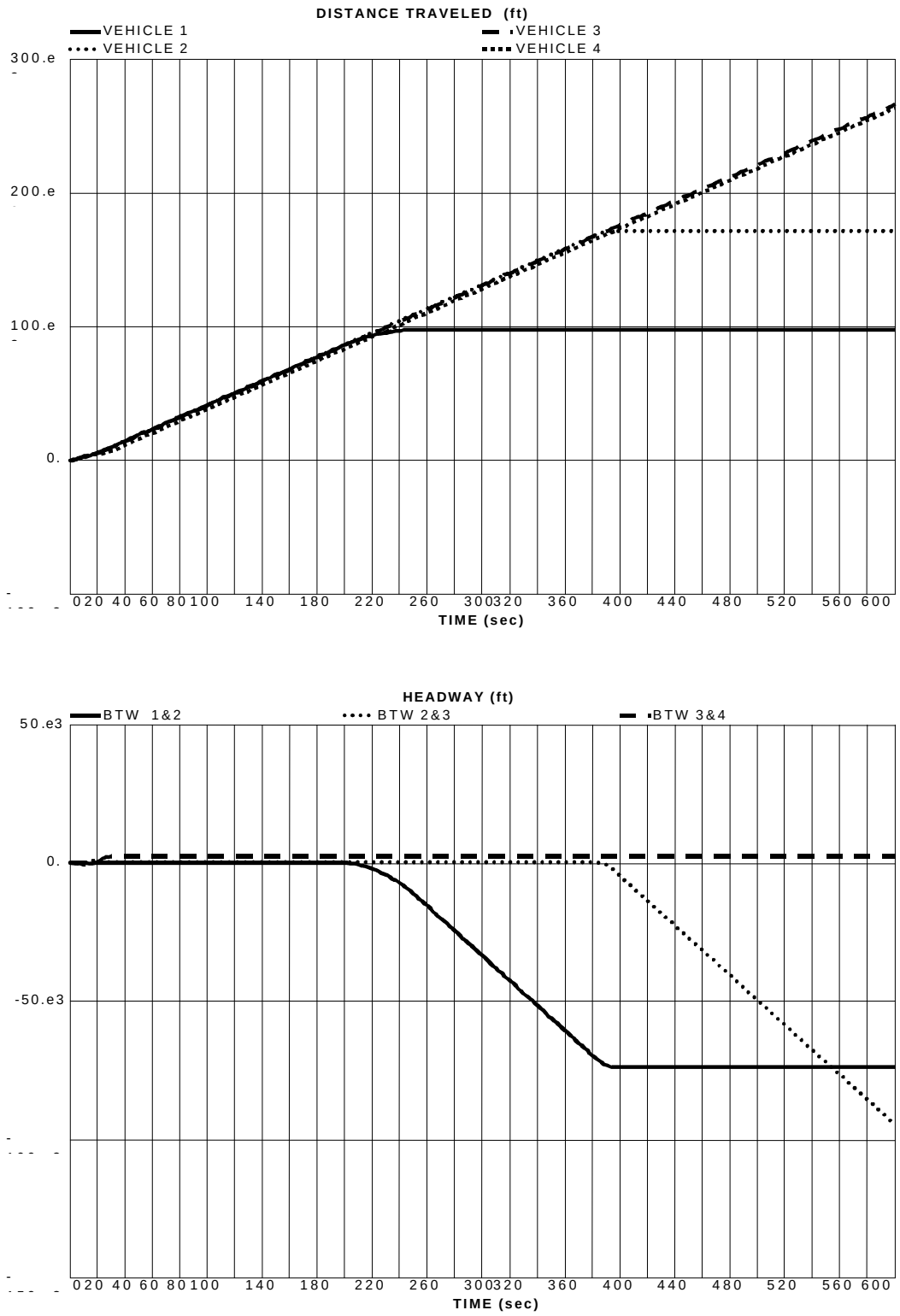

Figure 6.5a Vehicle Characteristics under Spacing Dependent Law (b = 0.01)

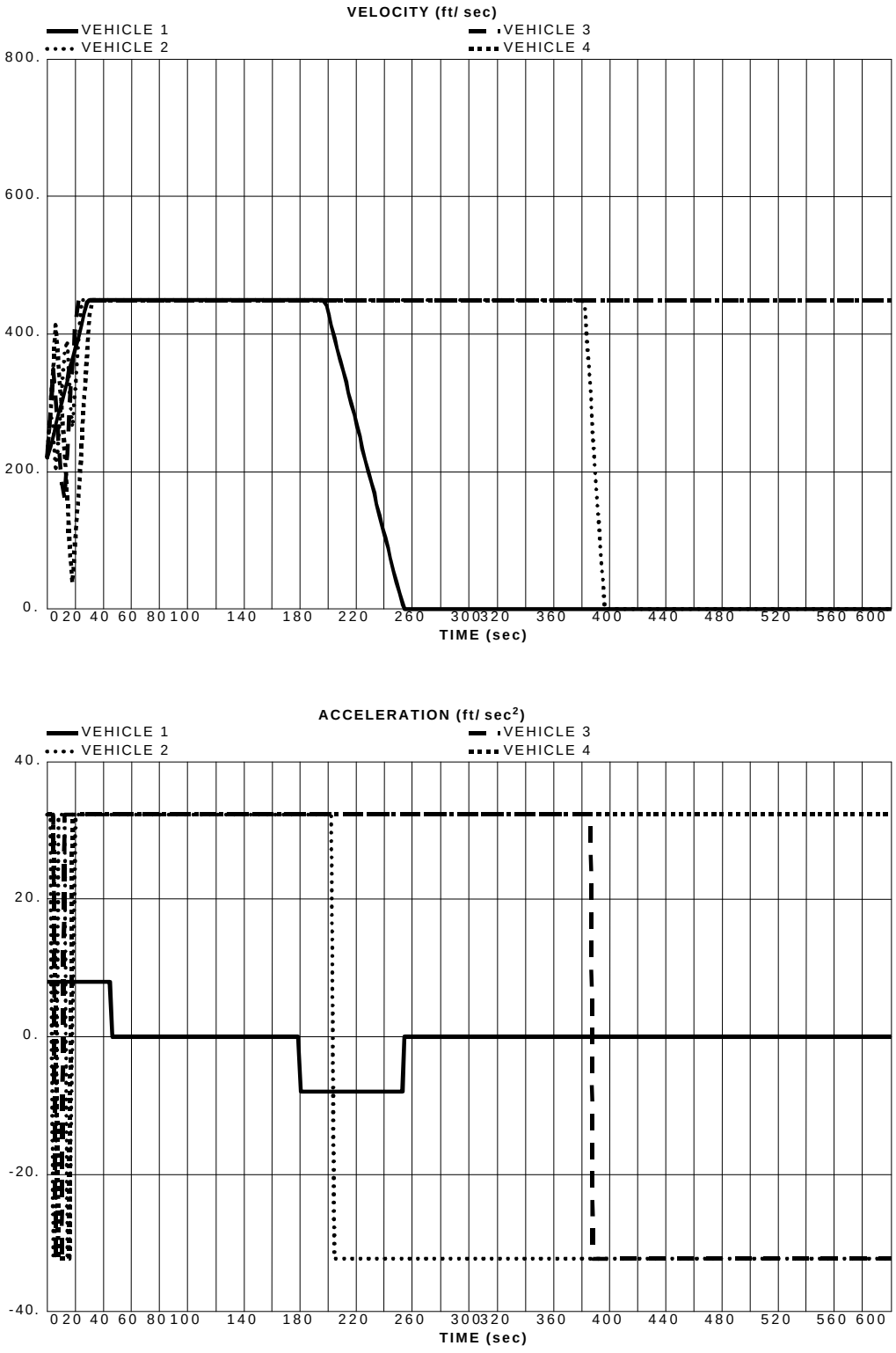

Figure 6.5a (cont'd) Vehicle Characteristics under Spacing Dependent Law (b = 0.01)

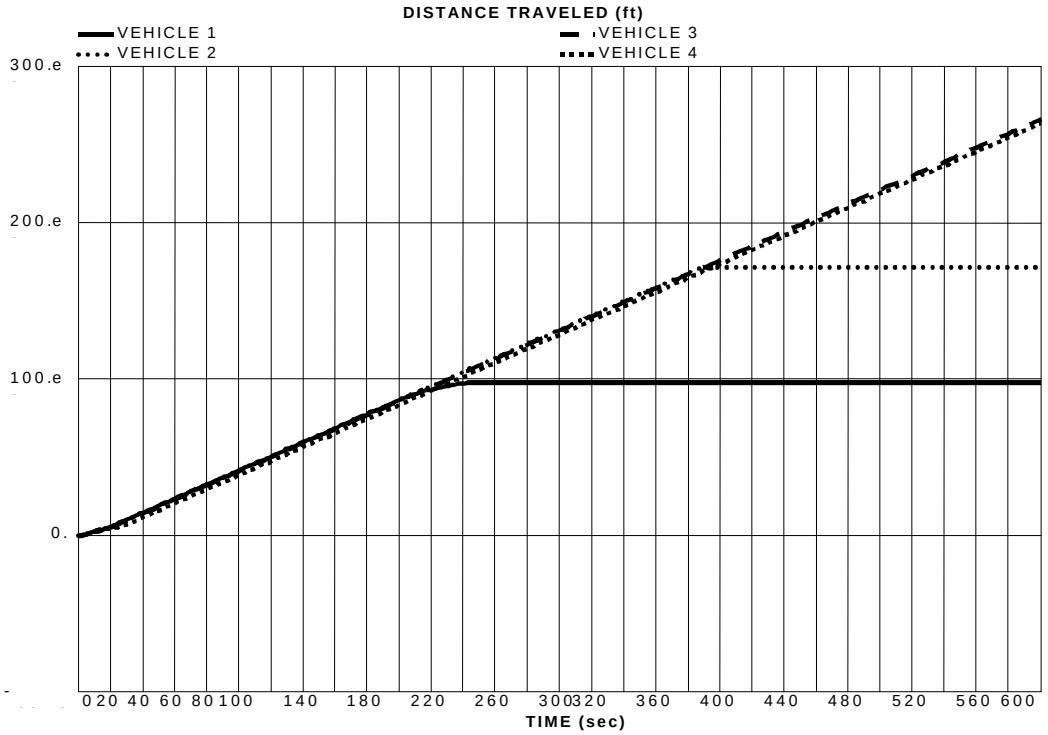

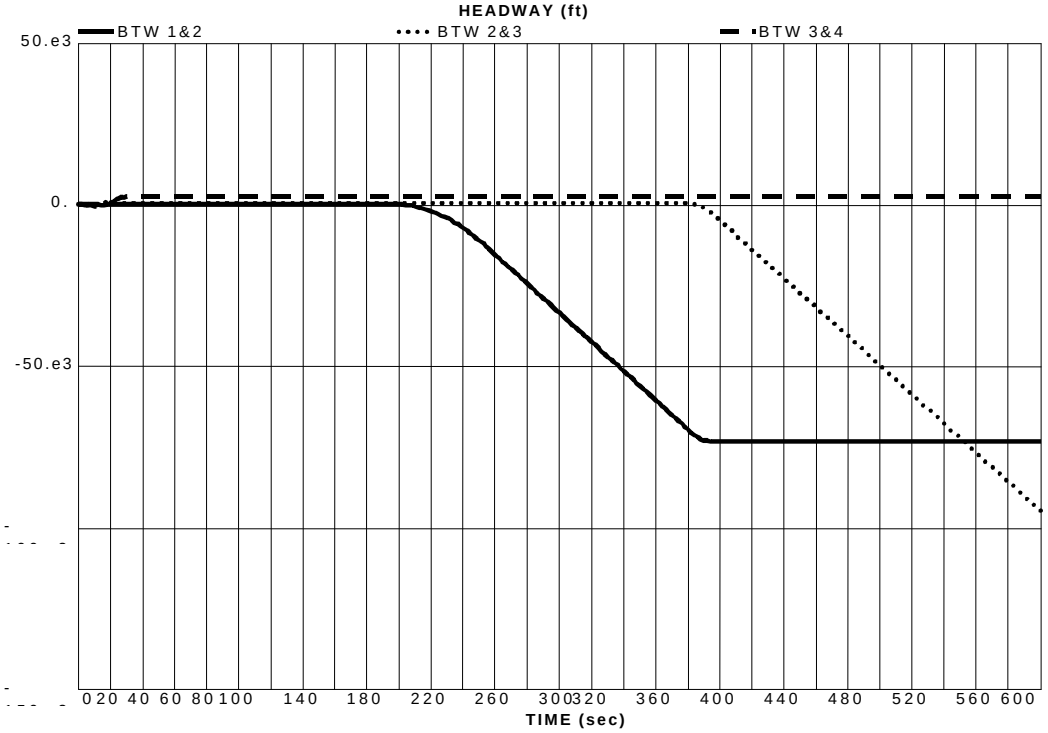

Figure 6.5b Vehicle Characteristics under Spacing Dependent Law (b = 0.005)

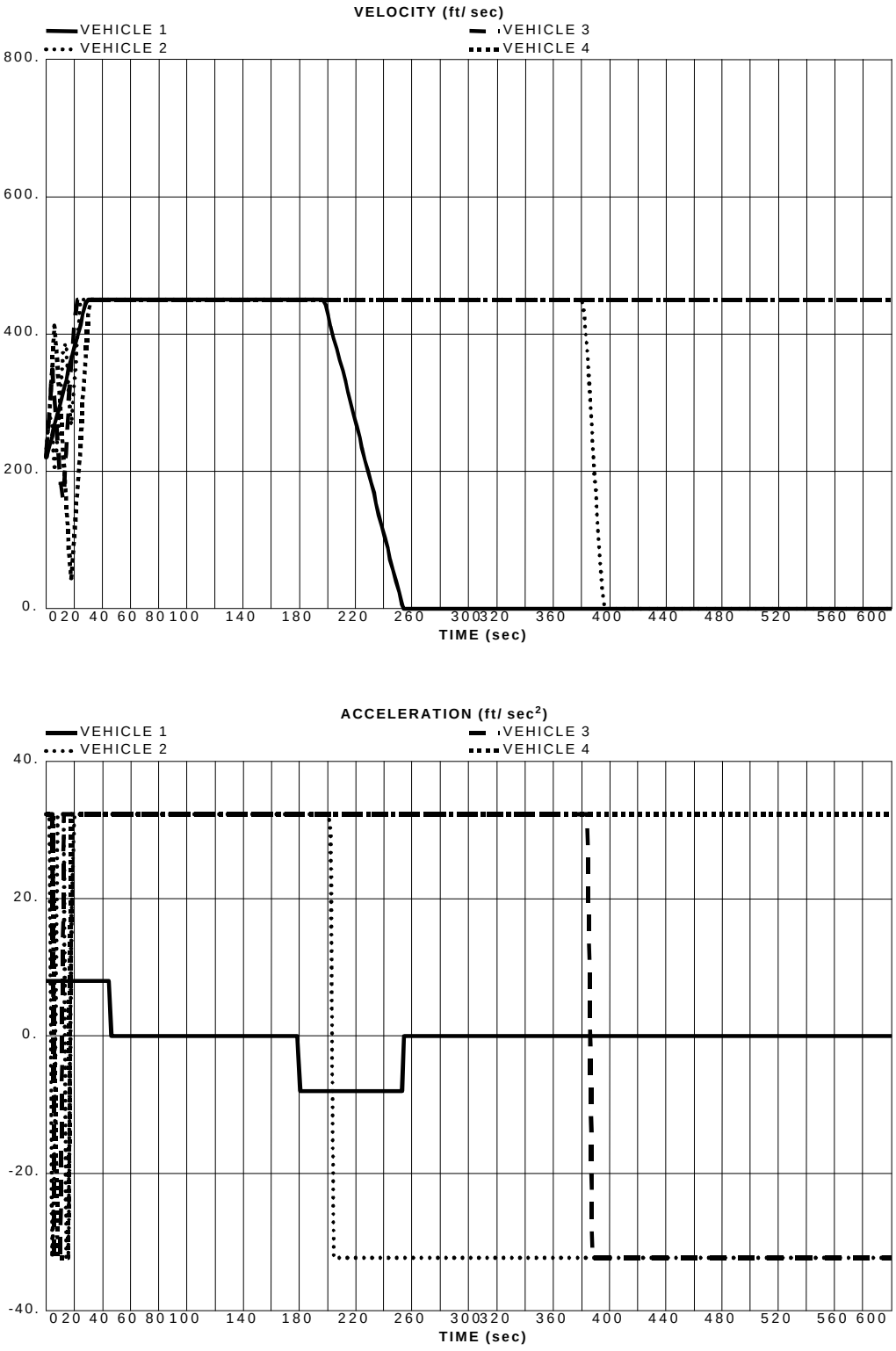

Figure 6.5b (cont'd) Vehicle Characteristics under Spacing Dependent Law (b = 0.005)

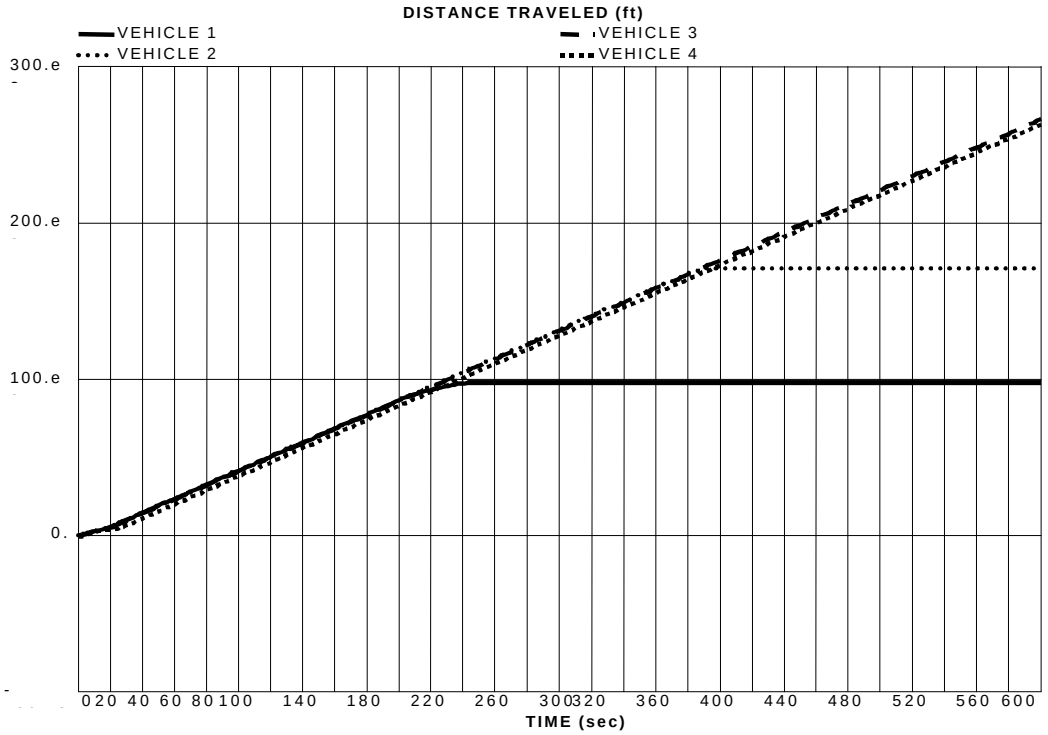

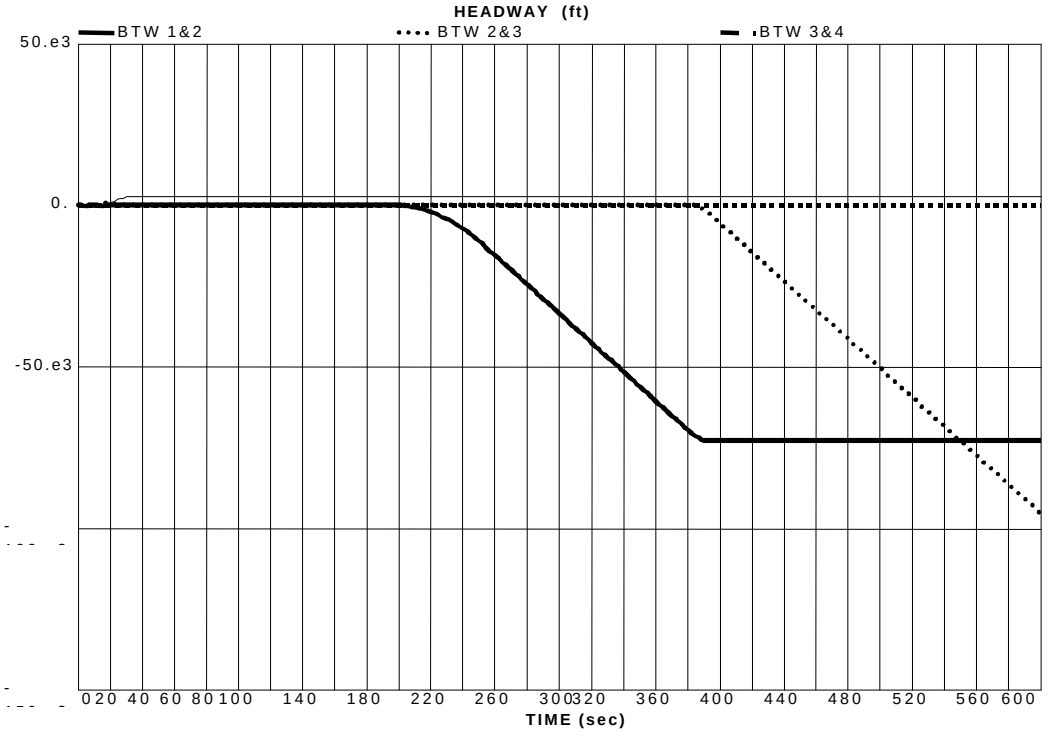

Figure 6.5c Vehicle Characteristics under Spacing Dependent Law (b = 0.001)

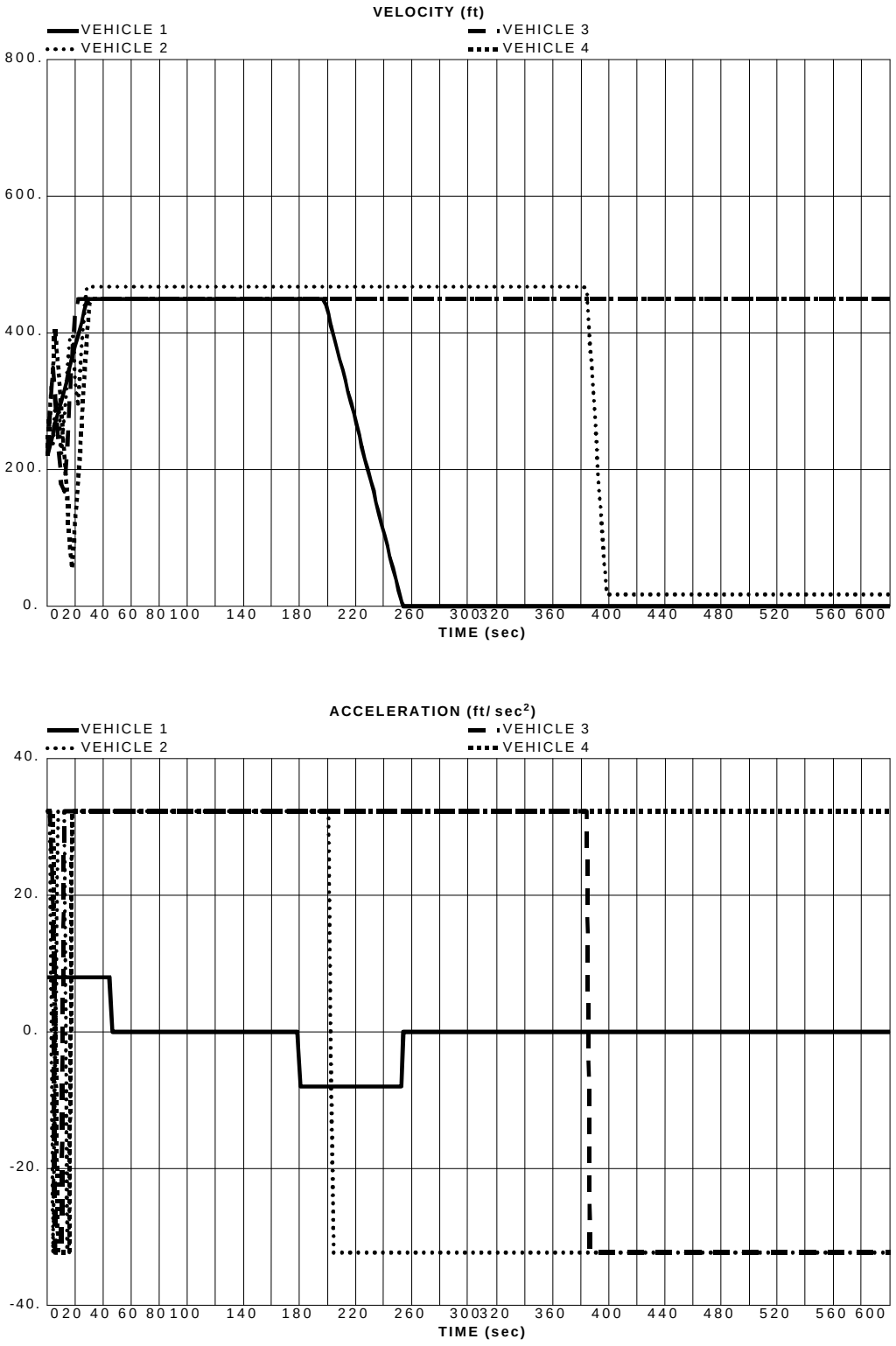

Figure 6.5c (cont'd) Vehicle Characteristics under Spacing Dependent Law (b = 0.001)

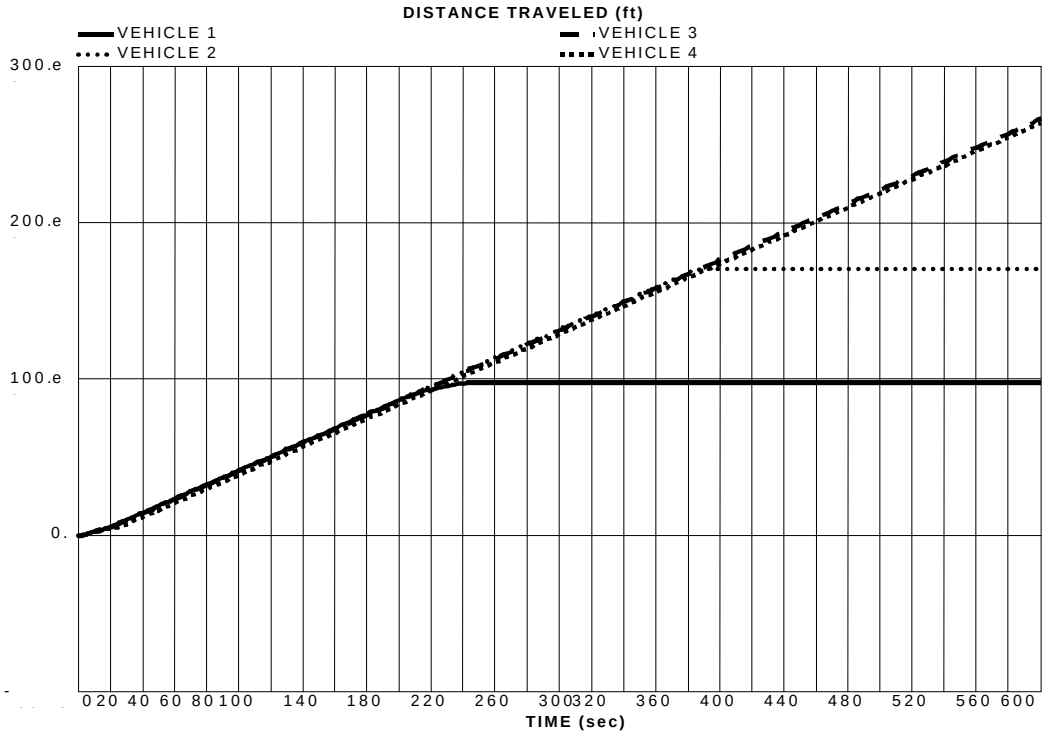

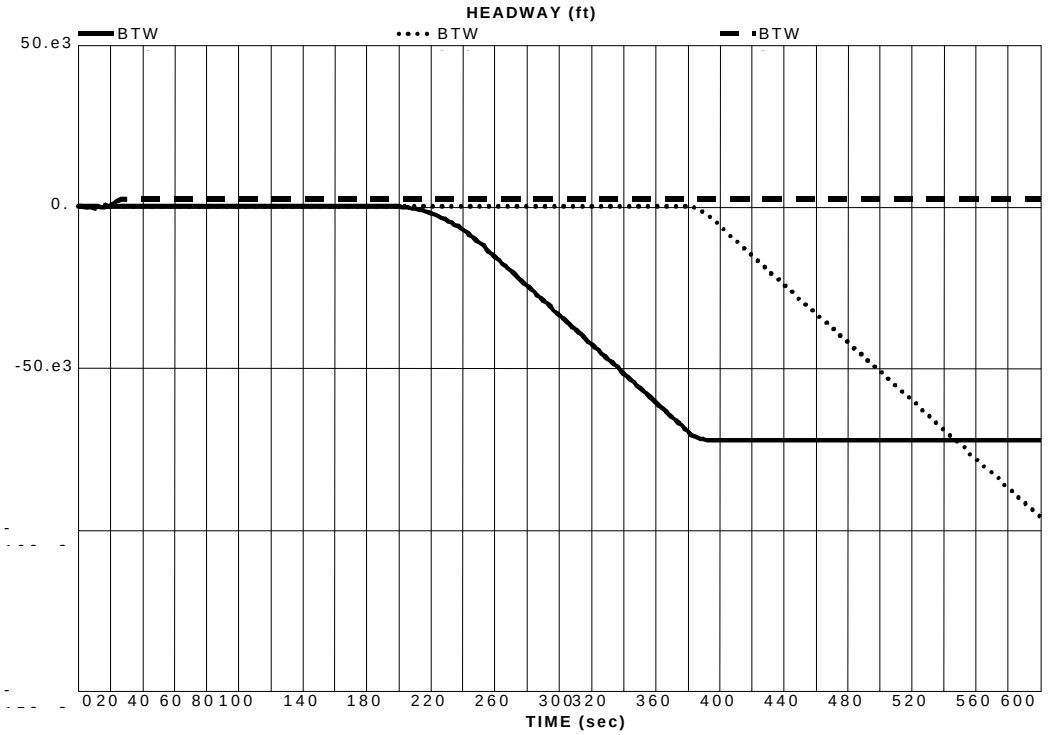

Figure 6.5d Vehicle Characteristics under Spacing Dependent Law (b = 0.0005)

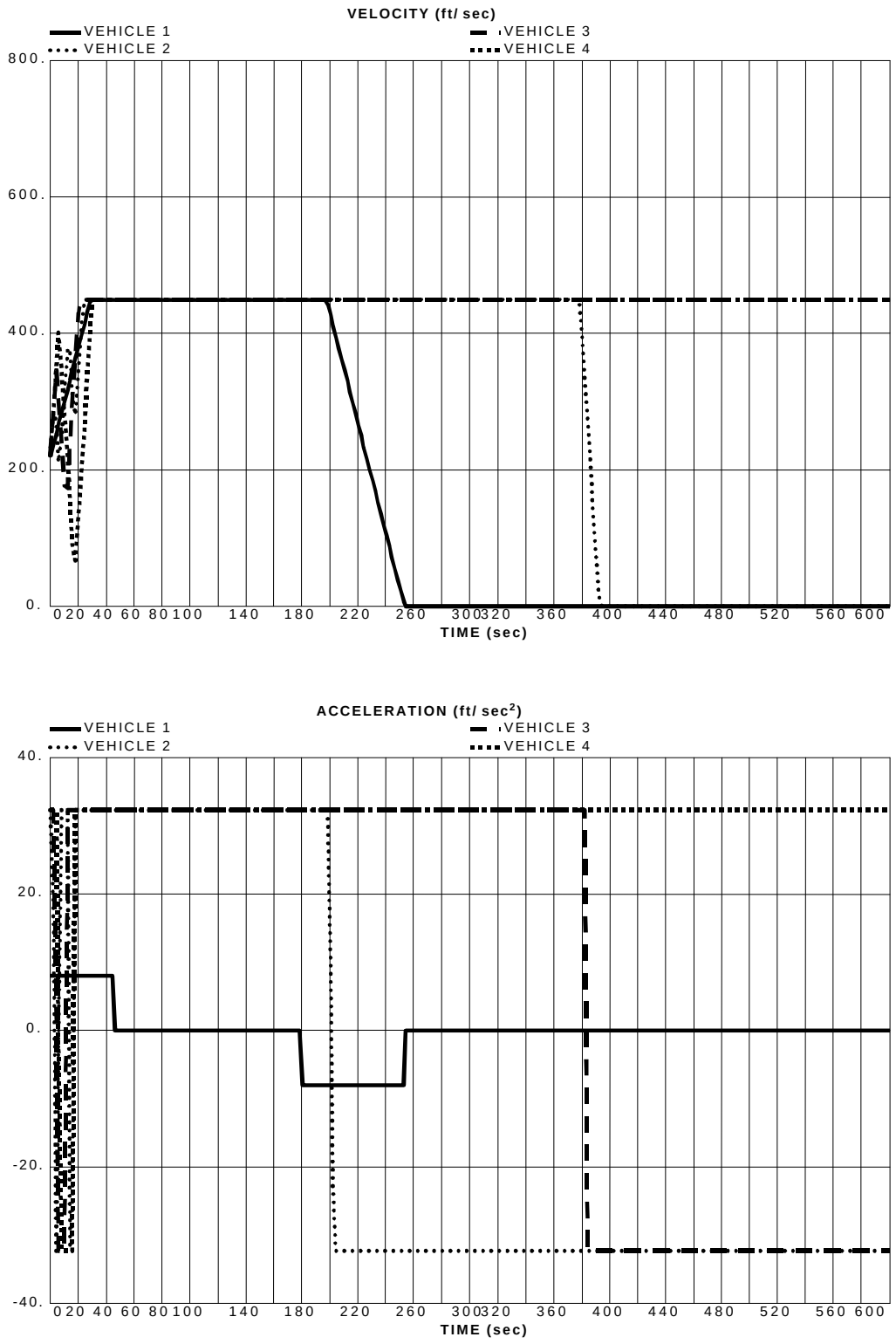

Figure 6.5d (cont'd) Vehicle Characteristics under Spacing Dependent Law (b = 0.0005)

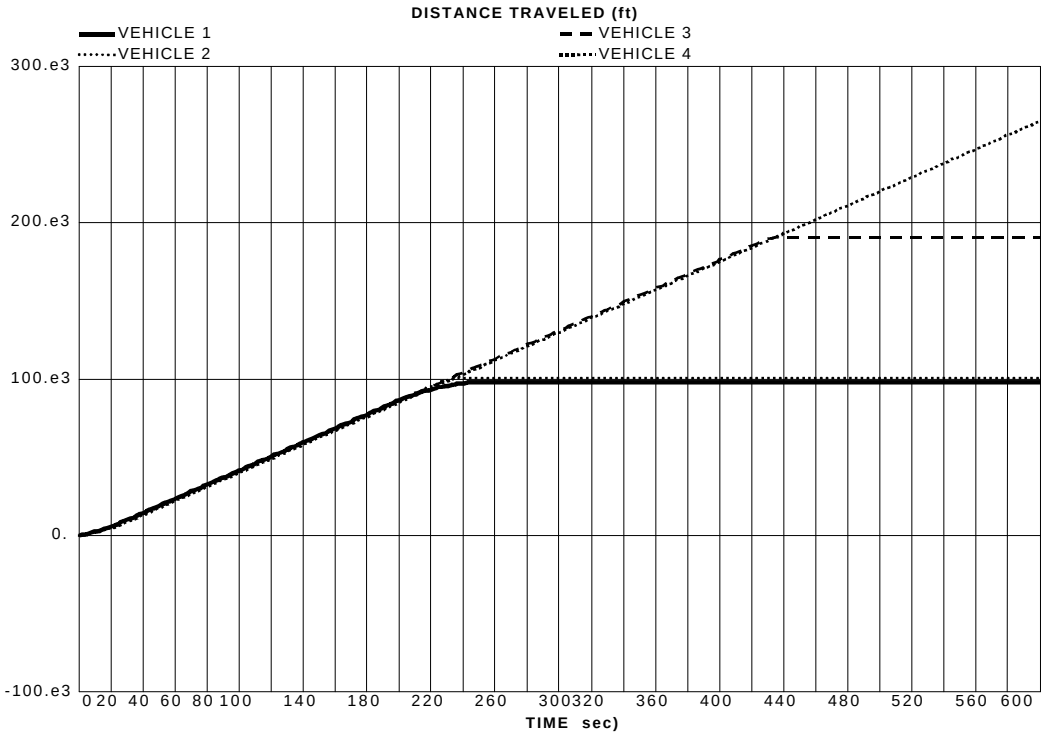

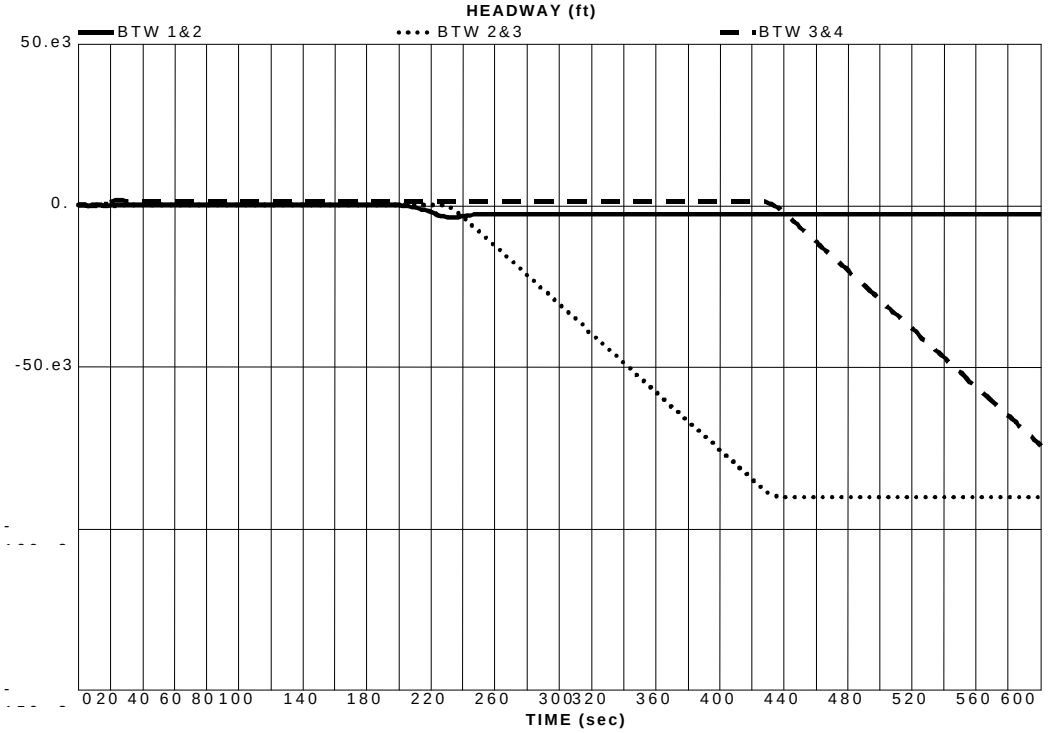

Figure 6.5e Vehicle Characteristics under Spacing Dependent Law (b = 0.0001)

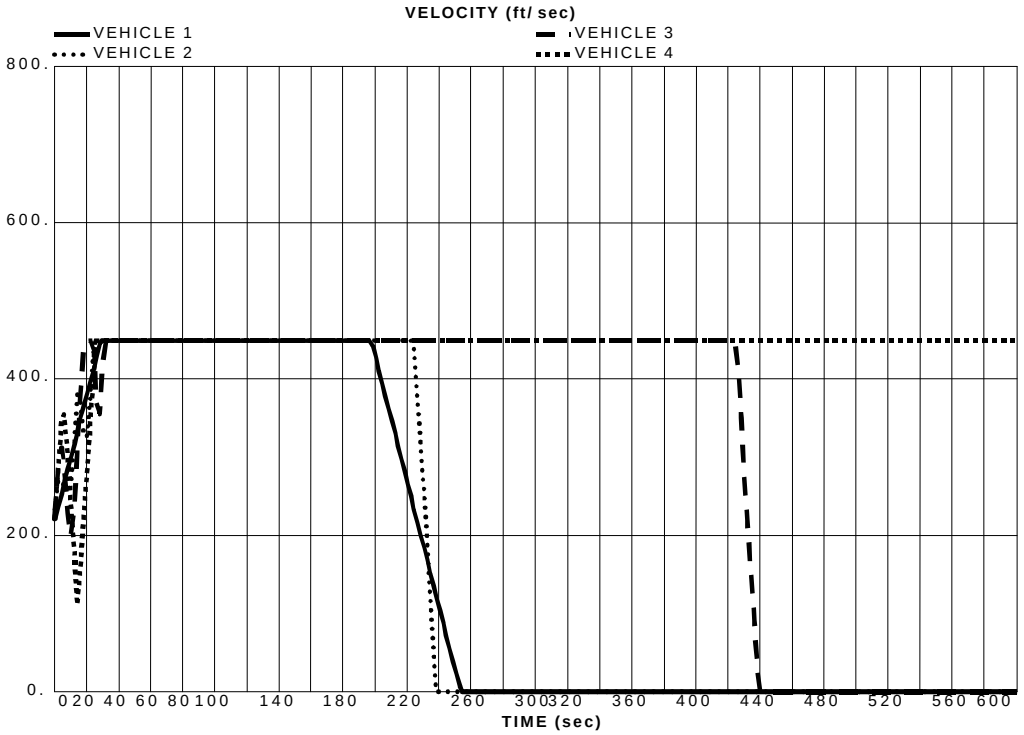

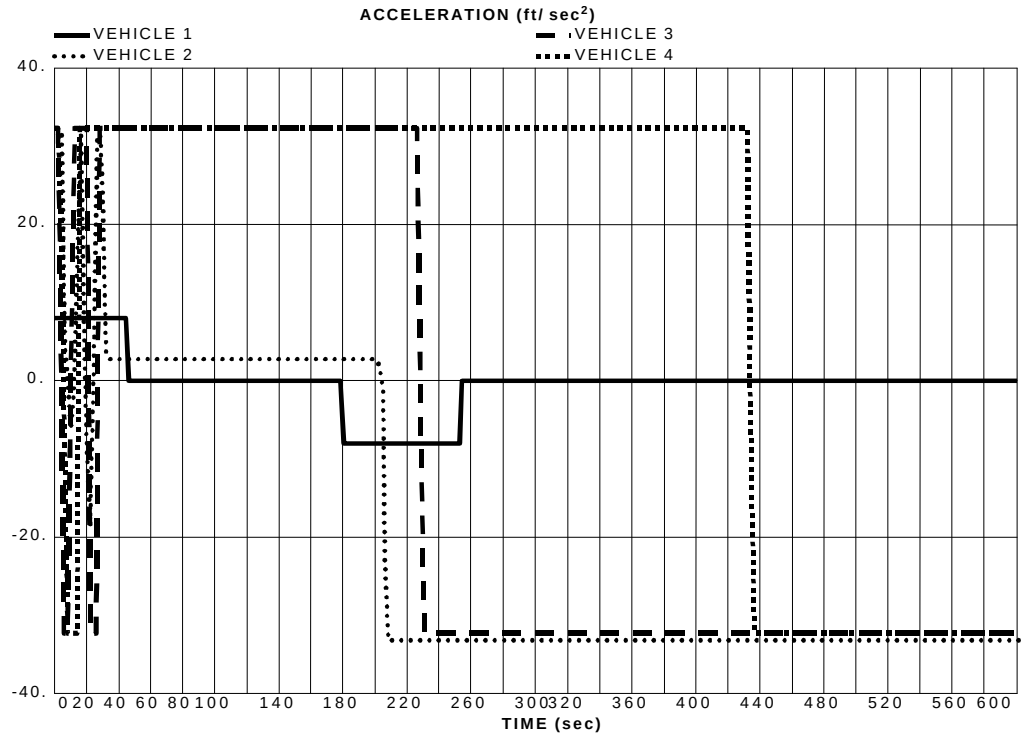

Figure 6.5e (cont'd) Vehicle Characteristics under Spacing Dependent Law (b = 0.0001)

6.7.3 Magnetic Coupling Control Model

Vehicles are considered a mass, which is suspended, guided, and propelled by a couple of forces that behaves like a spring system. The oscillation is an inevitable phenomenon, but can be limited to an acceptable level by adjusting magnetic and damping constants.

One can notice the difference in magnetic coupling model to that modeled in three-dimensional control law. Instead of focusing on headways between vehicles, each vehicle is modeled its trajectory, headway to its predecessor, velocities and acceleration individually. Similarly to what have been examined in Section 6.5, all the vehicles adjust themselves to a steady state after a short period of time. They follow each other while keeping constant close headways of 15 ft. Magnetic constants XK does not play a significant row in changing the vehicles' movement patterns since the vehicles start from almost identical speeds and accelerations. The simulation results are illustrated in Fig 6.6.

6.7.4 Combinations of Longitudinal Control Models

Each model consists of several decision variables, which are altered to investigate the possible critical headways, velocities and accelerations. A sensitivity analysis is utilized to study the effect of these variables in each longitudinal control model when applied individually.

Since each longitudinal control model has control rules that provoke different movement patterns, a model can be relevantly applied to an exact range of accelerations, speeds and headways. The combination of two or more models is designed to eliminate shortcomings of a single model. The combinations can be of two forms: stepwise and cooperated.

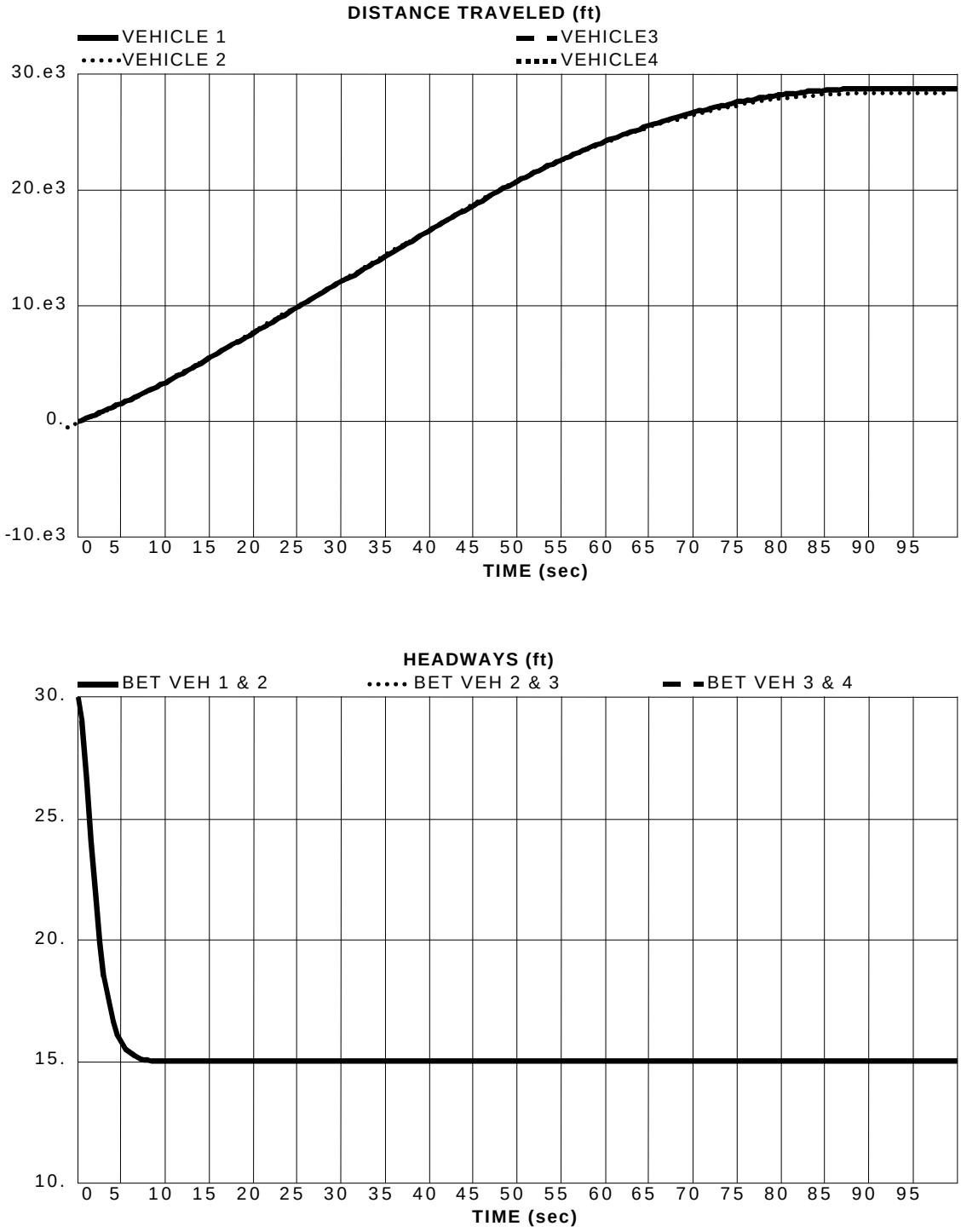

Figure 6.6 Vehicle Characteristics under Magnetic Coupling Control Law

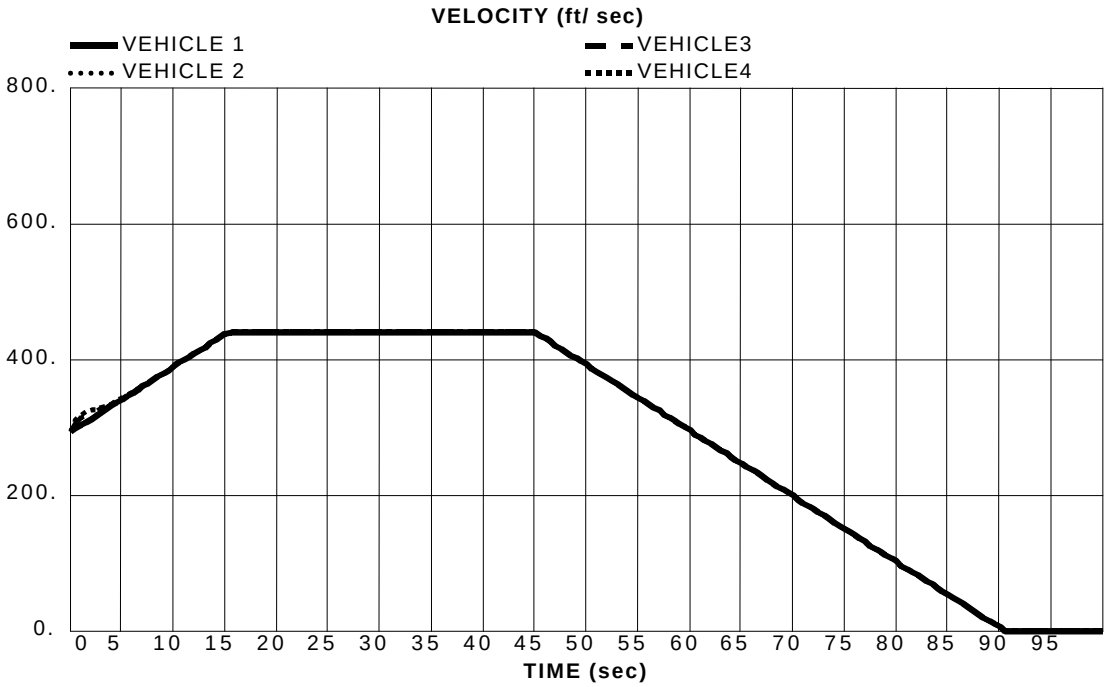

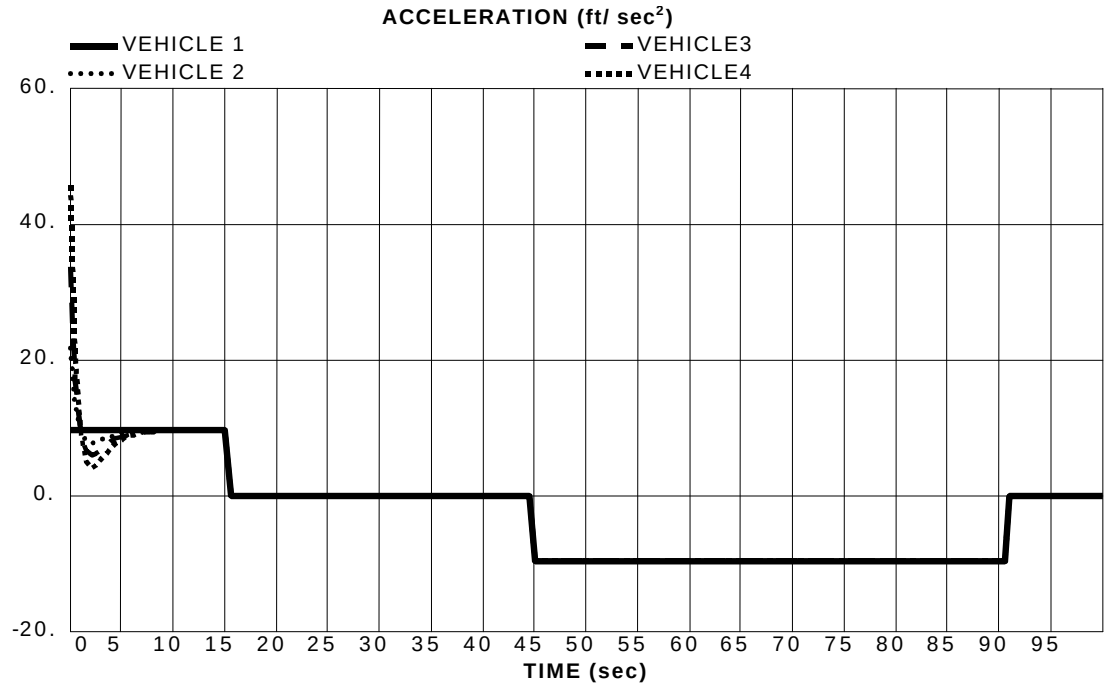

Figure 6.6 (cont'd) Vehicle Characteristics under Magnetic Coupling Control Law

Stepwise combination involves application of a single model over a range of speed or headway and switching to another model when the threshold changes. Since the speed differences are not as significant after a vehicle taking off to a cruising speed, the original proposal thresholds are different ranges of headways between vehicles.

The car maneuvering and spacing dependent models are used in the first interval where spacings between vehicles are too large for magnetic force to attract. The issue to be investigated is whether a step-wise or cooperation combination of the two models is more suitable for controlling the vehicles.

The stepwise control rule will be applied using spacing as thresholds. When a pair of vehicles has headway more than a particular distance S_p, which can be considered "platooned", the vehicles are governed by fluid analogy control law. After the vehicles come closer together than S_p, but not less than the distance that can be control under magnetic influence S_c, the control mode switches to spacing dependent rule. Eventually, when the spacing is reduced less than S_c, the magnetic coupling rule is applied. The mathematical expression of stepwise longitudinal control is referred to in equation 5.42. Figure 6.7 shows the trajectory, speed, and acceleration characteristics of vehicles under stepwise control rule.

Under such stepwise control rule, the vehicles still come to a collision after some period of time, regardless of parameter selection. Fluctuations of velocities and accelerations still remain, although they are not as strong as those are from applying a single model. This could be due to the discontinuity of acceleration changes during switching between fluid analogy and spacing dependent modes of control.

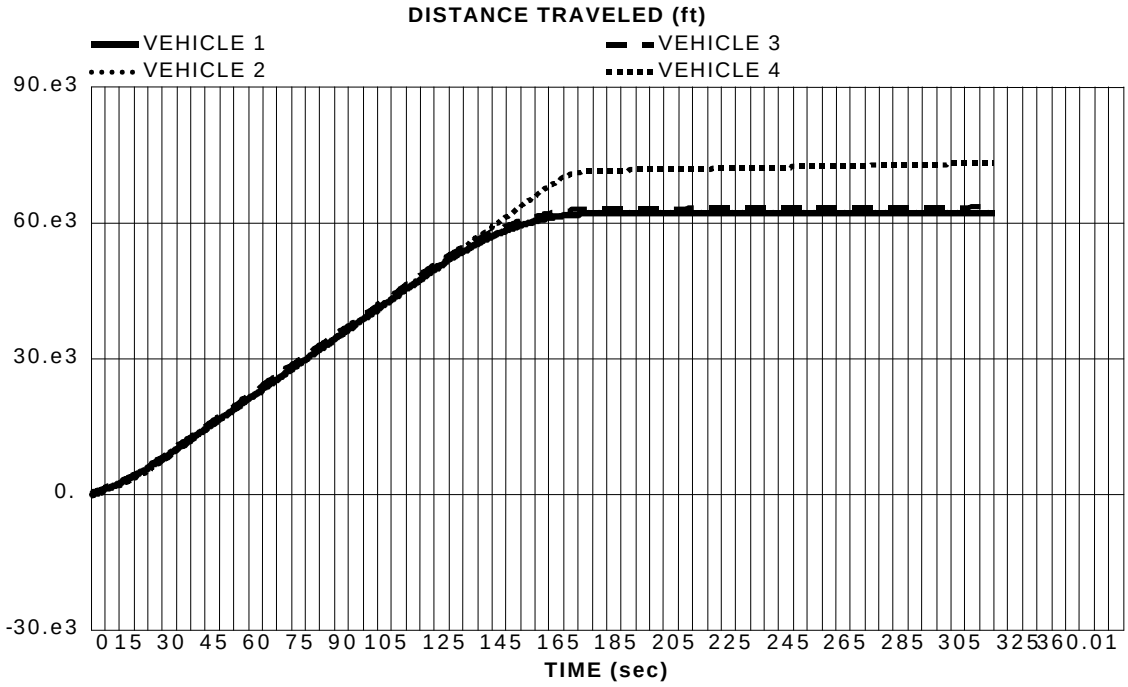

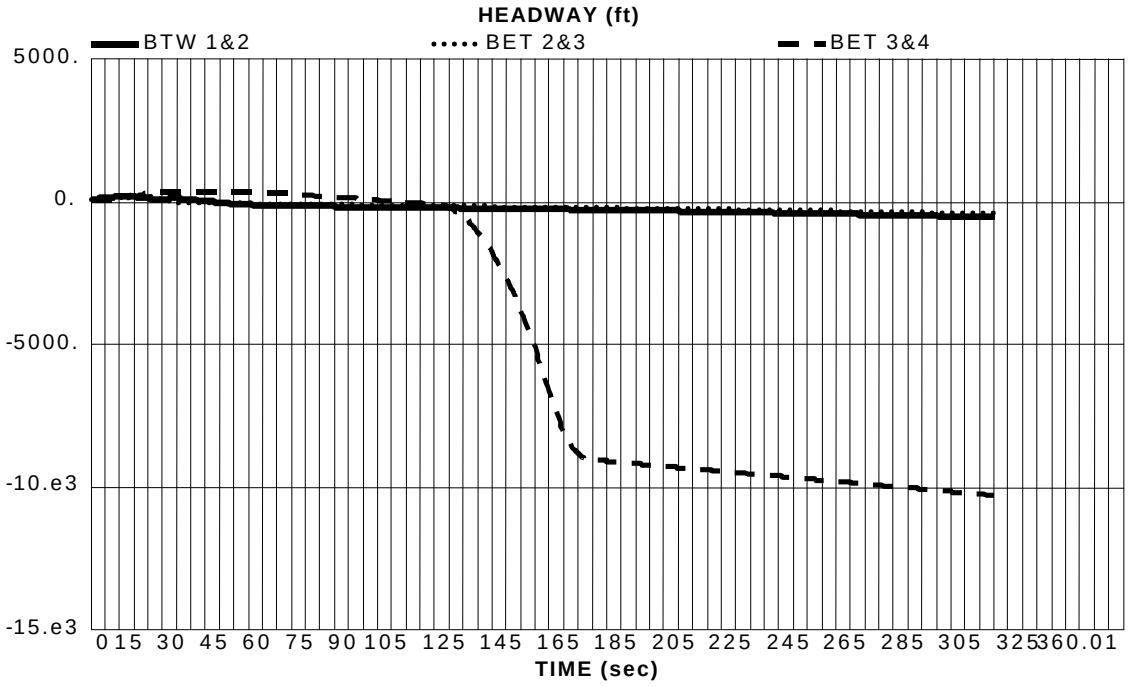

Figure 6.7 Vehicle Characteristics under Stepwise Longitudinal Control Law

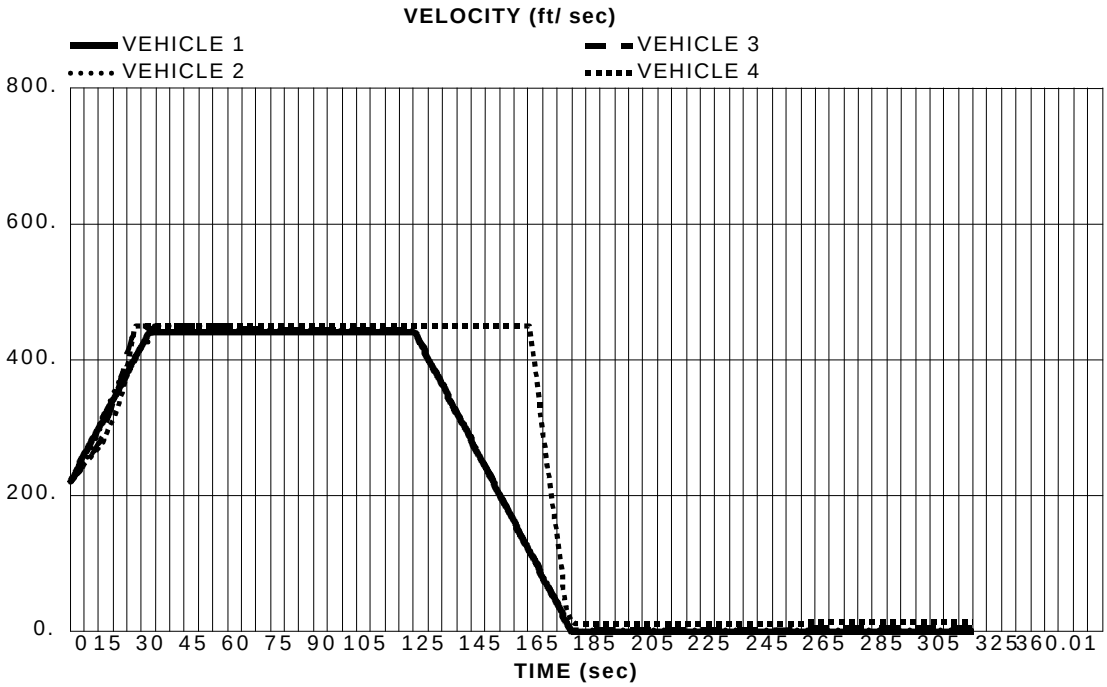

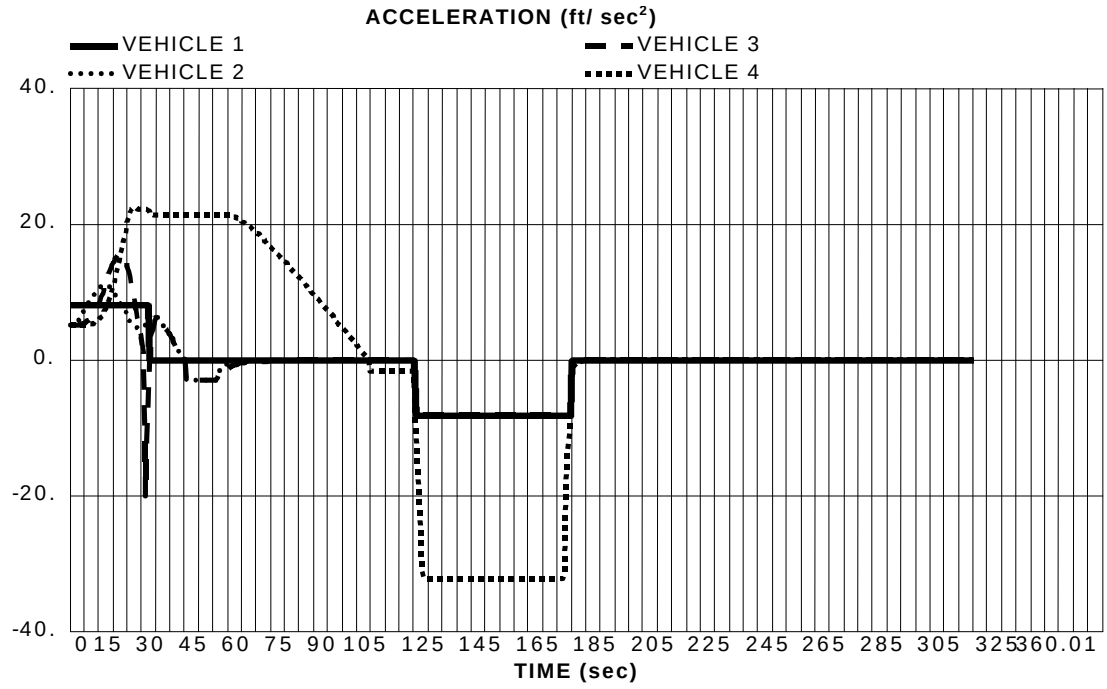

Figure 6.7 (cont'd) Vehicle Characteristics under Stepwise Longitudinal Control Law

Cooperation of the two models can be executed. The combination of the fluid car-following model and the spacing dependent model, as recommended by Addison and Low is believed to reduce the asymptotic instability [71]. The proposed longitudinal control law is expressed as:

$$\ddot{x}(t) = \begin{cases} -c^2 k_{i-j,i+p}(t-T)(\partial k/\partial x)_{i-j,i+p} + b[x_{i-1}(t-T) - x_i(t-T)] & x_{i-1} - x_i \geq S_c \\ XAP(t) - XAD(t) & x_{i-1} - x_i \leq S_c \end{cases} \tag{6.50}$$

By mean of sensitivity analysis, the following parameters are assigned the values as follows: reaction time T = 0.05 seconds, S_p = 1320 feet, S_c = 50 feet, initial safe following distance = 100 ft, free flow speed u_f = 450 mph, jam density = 660 vehicles per mile per lane, b = 0.0001, l = 3, magnetic constant XK = 400 lbs/ft, and damping constant XD = 550 lbs/ft. The results of the simulation are shown in Figure 6.8.

6.8 Vehicle Motion in Curve

Since the Maglev guideway is designed to be integrated with the existing highways, radii of the curves should follows the same characteristics. Conservatively, the "Green Book" [80] suggested using maximum superelevation rate e = 0.04, and minimum coefficient of friction f = 0.09 for a design speed of 80 mph. Thus the curve radius is computed as

$$R = \frac{V^2}{15(e+f)} \tag{6.51}$$

$$= \frac{80^2}{15(0.04+0.09)} \approx 3280 \text{ ft}$$

where V is a design speed in mph.

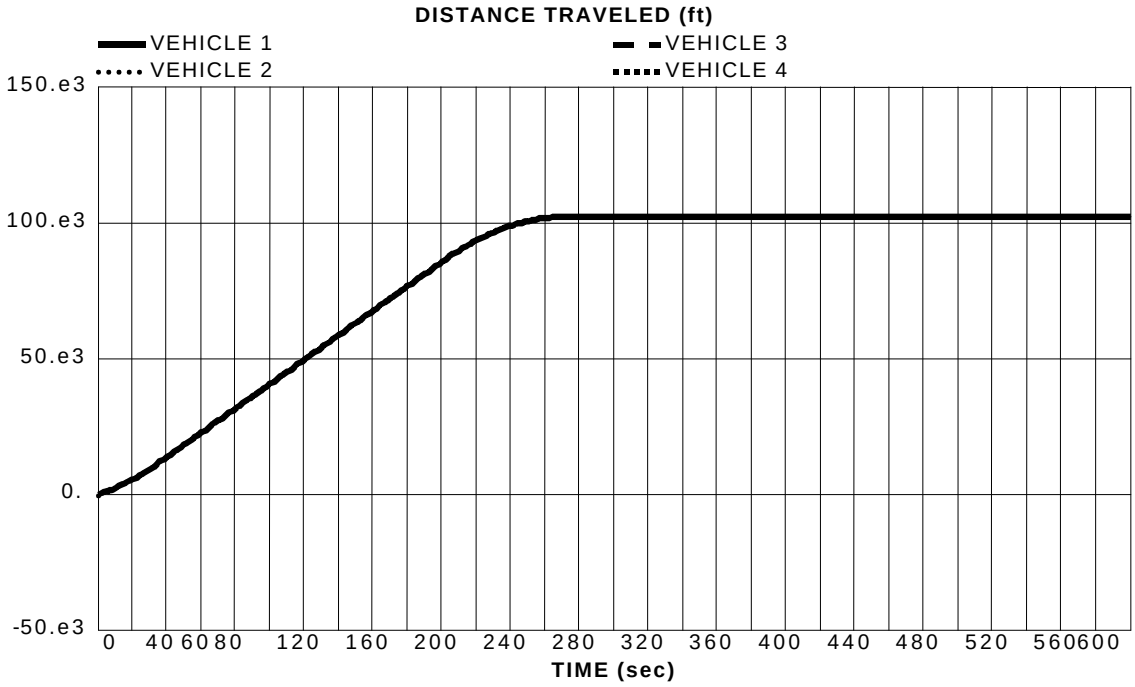

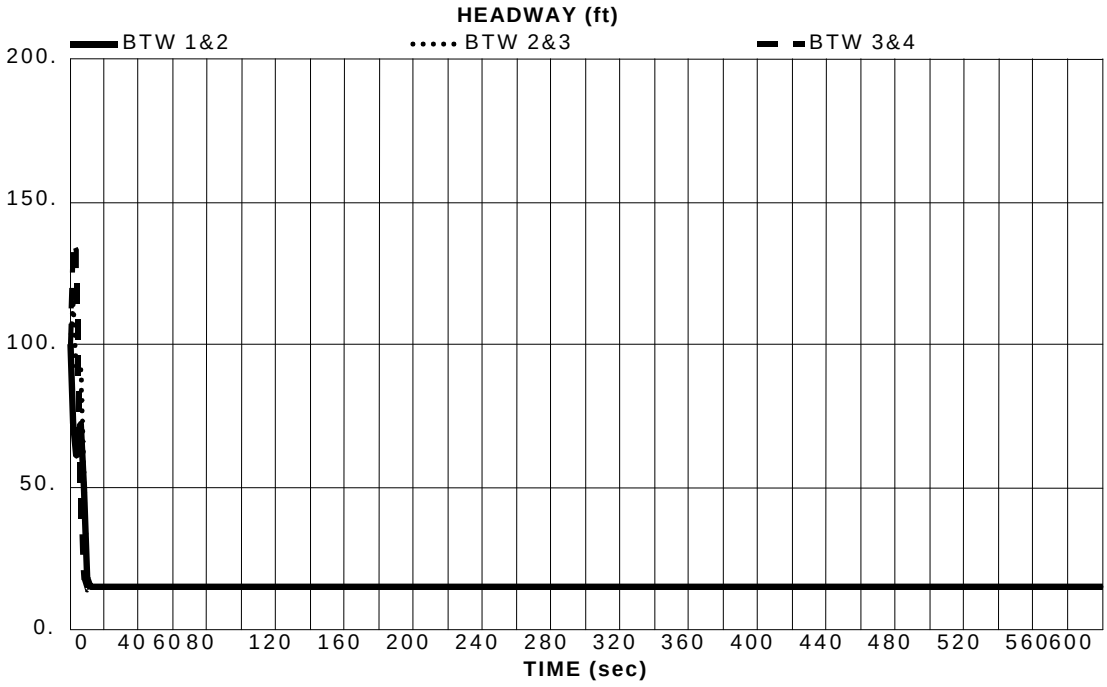

Figure 6.8 Vehicle Characteristics under Cooperative Longitudinal Control Model

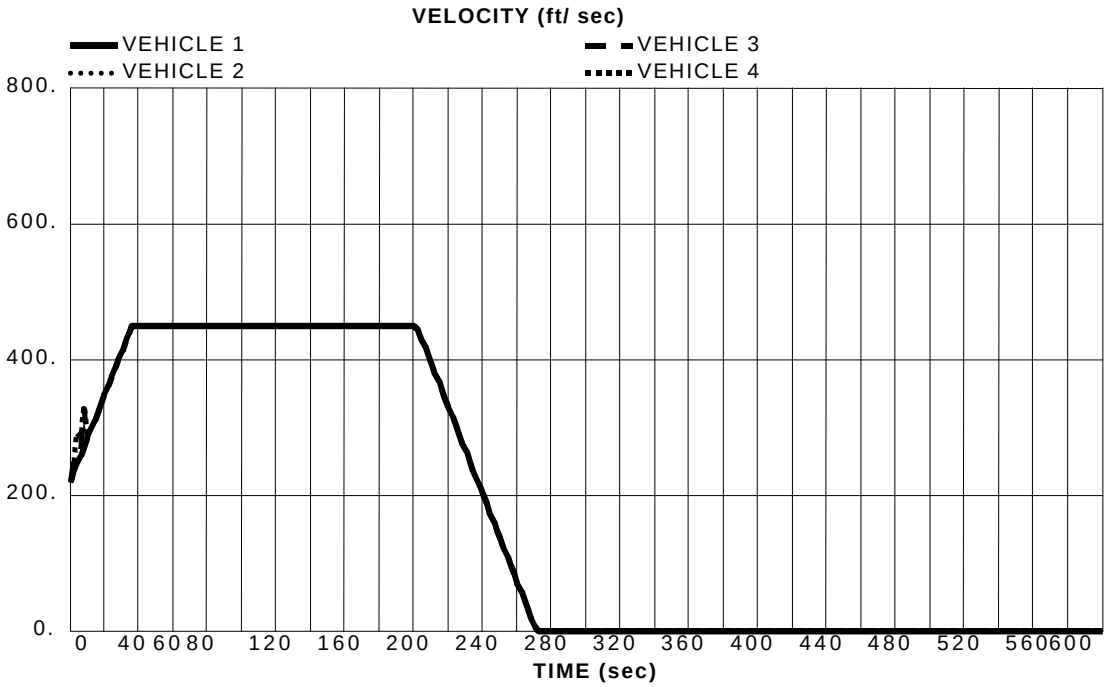

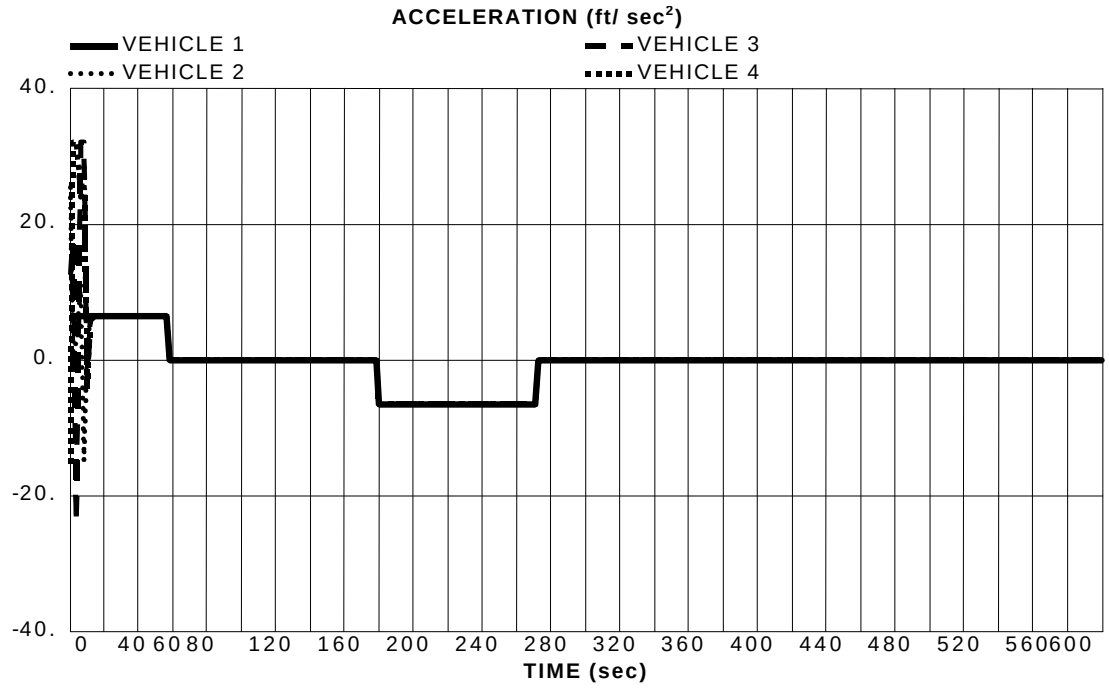

Figure 6.8 (Cont'd) Vehicle Characteristics under Cooperative Longitudinal Control Model

The use of spiral curves provides smooth transition of motions between a tangent section and a circular section. The radius of a spiral curve changes linearly from zero at the point of tangent *PT* to radius at the circular curve, with respect to the distance from *PT*. A mathematical relationship between the spiral curve length *L* and the curve radius *R* of such clothoids can be expressed as:

$$\frac{1}{R} = \frac{1}{R_C} \cdot \frac{L}{L_S} \tag{6.52}$$

where R_C is the circular curve radius and L_S is entire length of the spiral curve. This leads to a computation for spiral curve length, based on a centripetal acceleration of 2ft/s^2, as follows [80]:

$$L_S = 1.6\frac{V^3}{R} \tag{6.53}$$

$$= 1.6 \times \frac{80^3}{3280} \approx 250 \text{ ft}$$

Operating at high speeds, a Maglev vehicle will be traveling on curves with a steep 30-degree superelevation rate. The vehicle in a curve is tilted with an angle change 3 degrees per second, which is comparable to a standard turn rate of aircraft. With advance in tilted technology, a maglev vehicle will gradually tilt itself before entering the spiral curve in order to reduce the impact of centripetal force. The vehicle is expected to tilt up to 10 degrees before entering the superelevated section, thus results in aggregated angle of about 40 degrees, which is comparable to that of high-speed rail systems.

A model is constructed to illustrate a vehicle entering a 90-degree curve. The critical direction to control, however, is not on the lateral axis (Y-axis), but on the vertical axis (Z-axis) since it has a smaller cushion between the vehicle and the guideway. Magnetic suspension and damping constants have to be slightly stronger than those used in straight section operation. This simulation uses 2000 lb/ft and 1220 lb/ft for magnetic and damping constants respectively. As shown in Fig 6.9, the vehicle can operate at as high speed as 250 mph without colliding with the guideway surface.

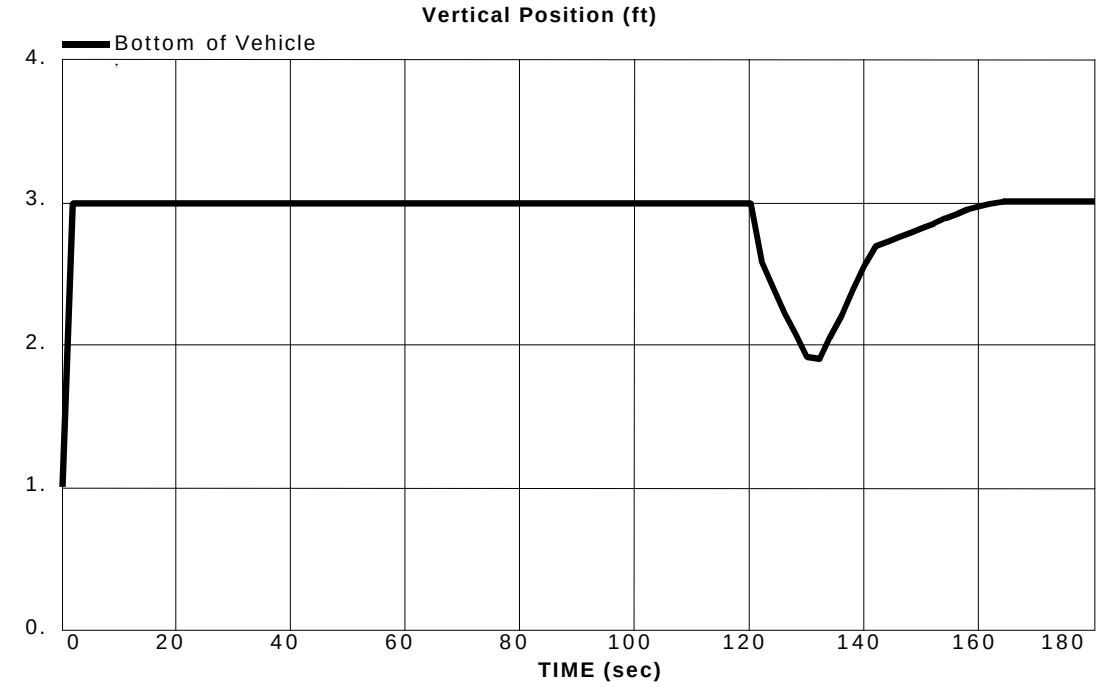

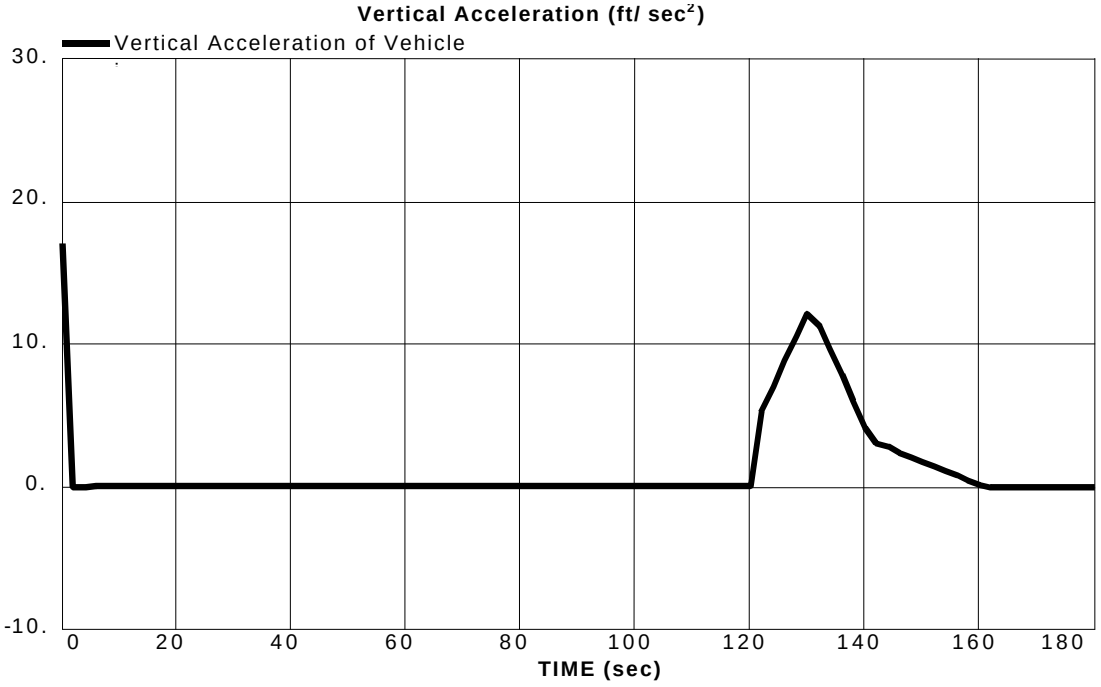

Figure 6.9 Vehicle Motion on a 90-Degree Curve

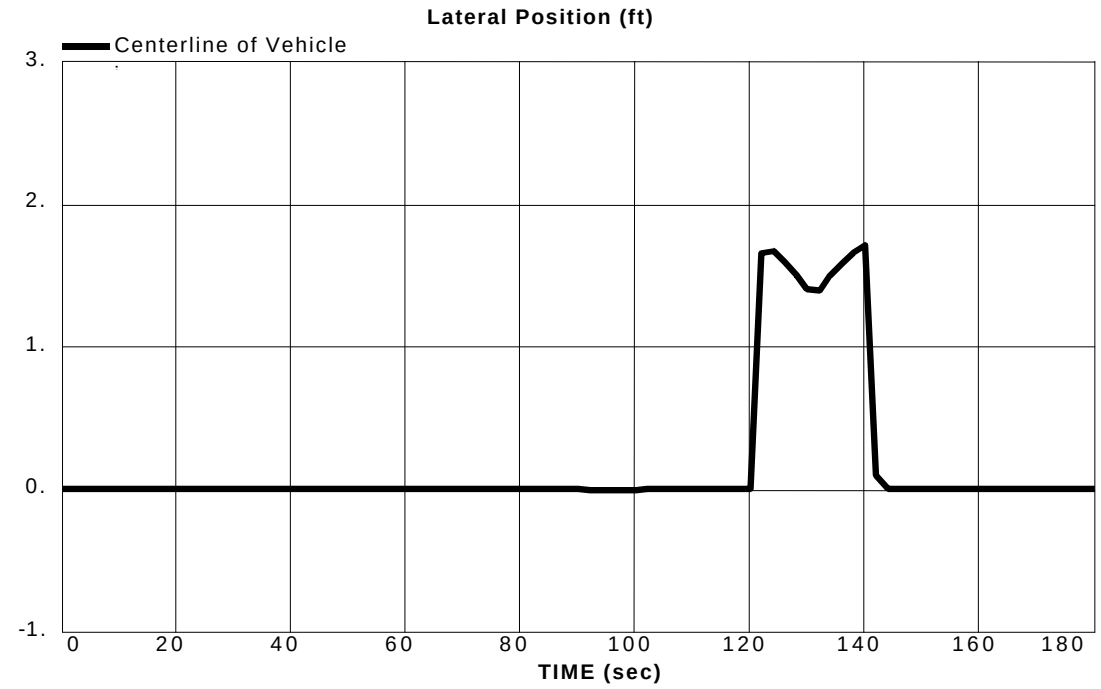

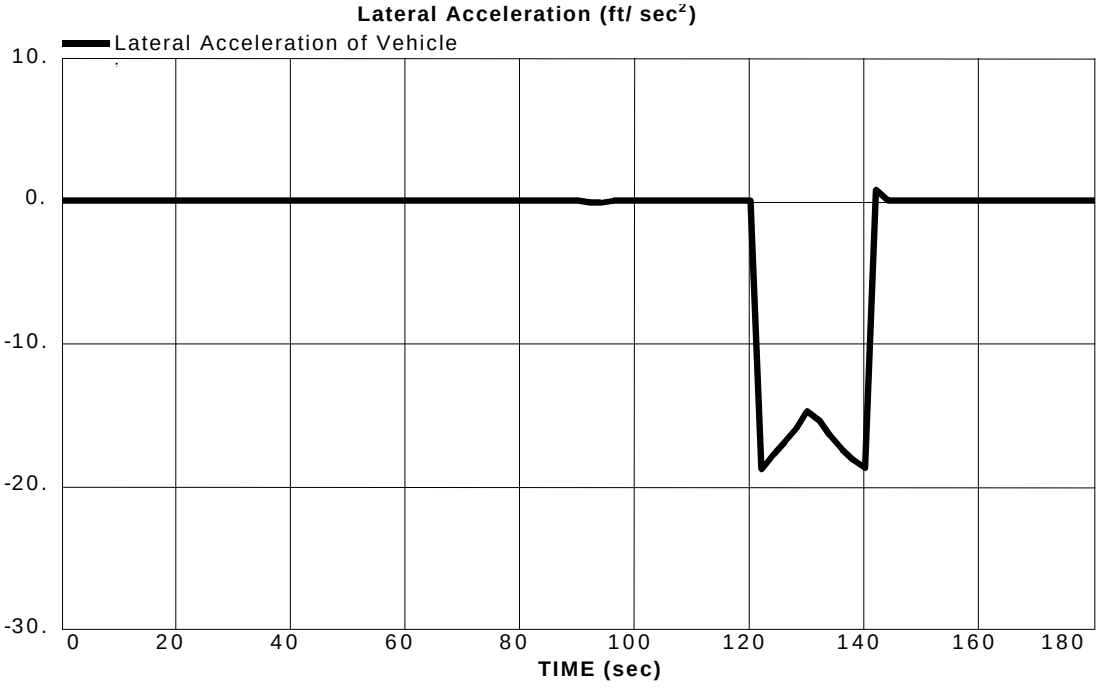

Figure 6.9 (cont'd)Vehicle Motion in a 90-Degree Curve

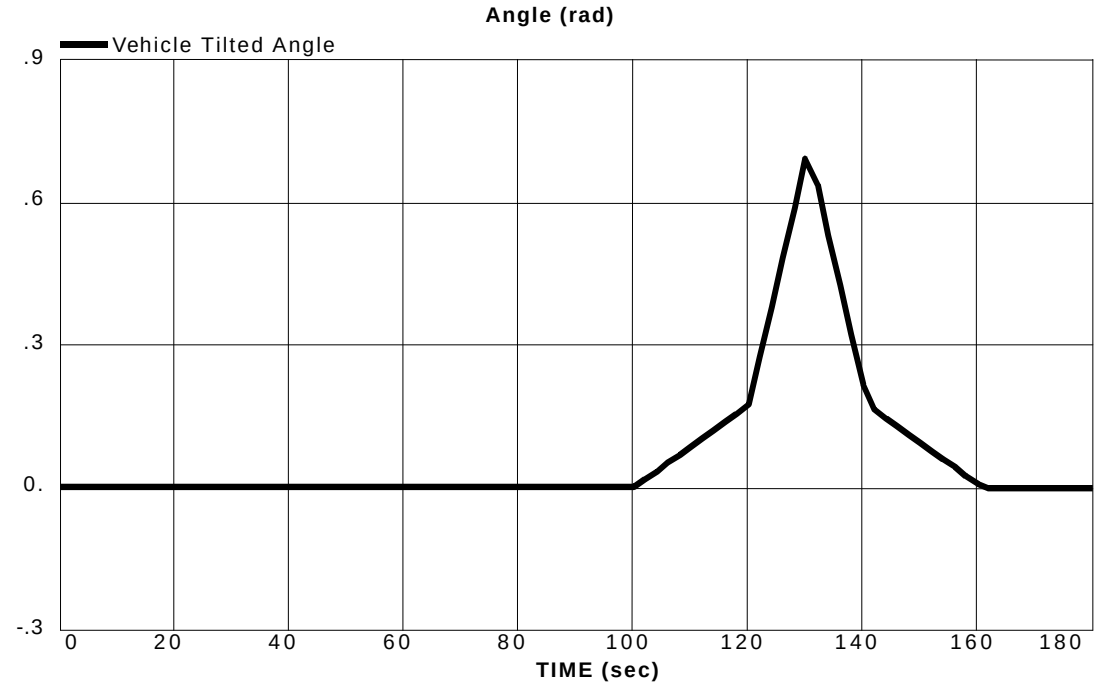

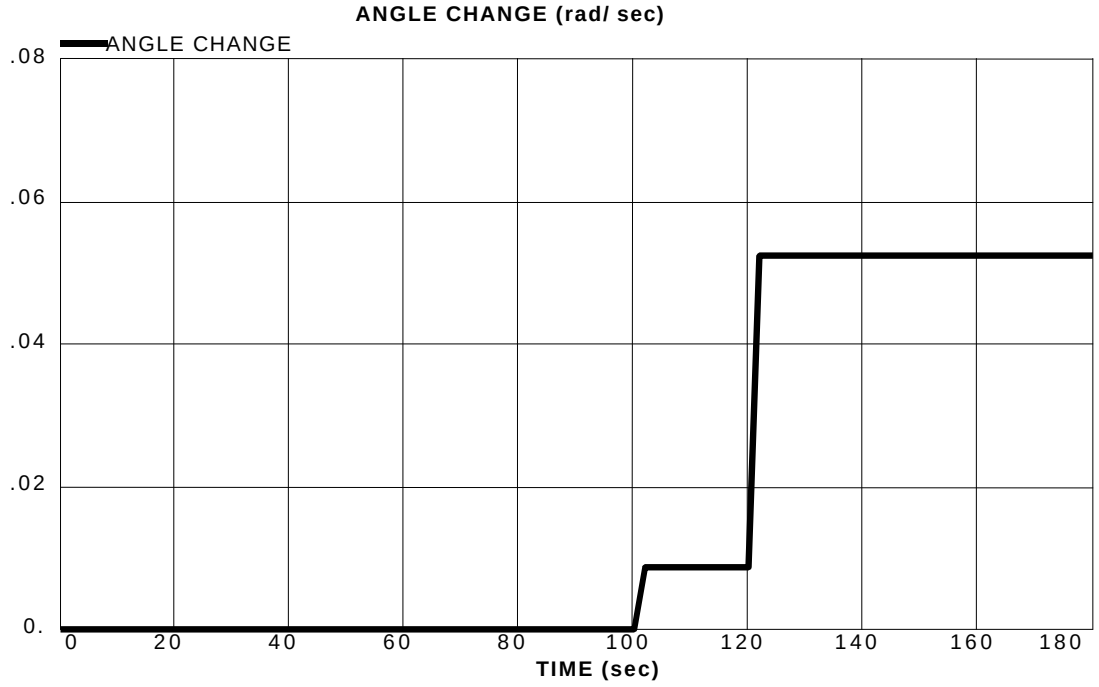

Figure 6.9 (cont'd) Vehicle Motion in a 90-Degree Curve

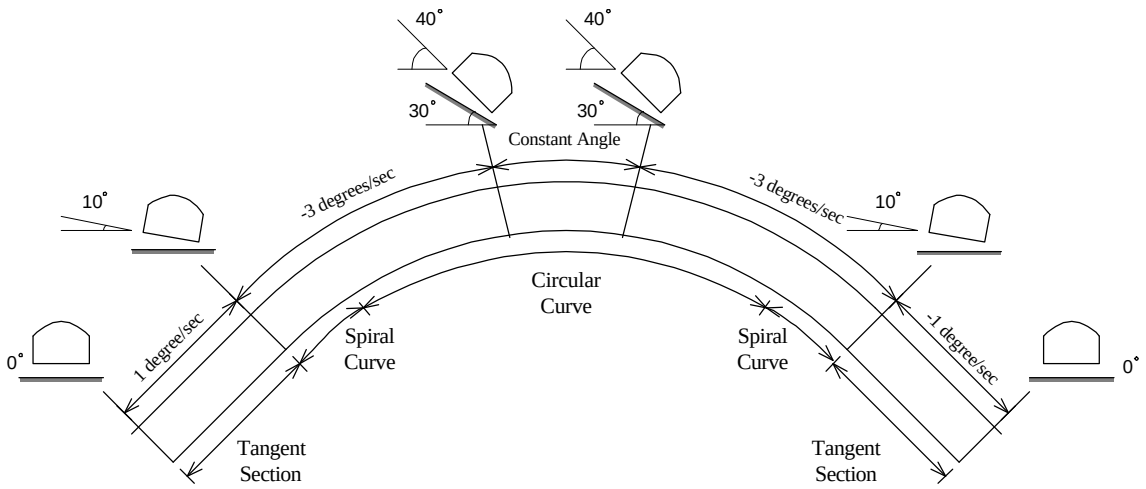

Figure 6.10 Vehicle Tilting and Superelevation in a Curvature Motion

6.9 Integration of 3-D Models

A complete vehicle position control scheme is obtained by integrating a simple 3-dimensional control scheme, a longitudinal control scheme and a circular motion control scheme. The complete model consists of four vehicles taking off the ground and adjusting their elevations, lateral position and headway to the desired positions. Then, the leading vehicle decelerates to adjust its velocity before entering a 90-degree curve. The following vehicles also adjust their speed according to the proposed longitudinal control rule (Equation 6.50).

The DYNAMO models in this chapter are included in Appendix A and the results of simulation are shown in Figure 6.11, 6.12, 6.13 and 6.14.

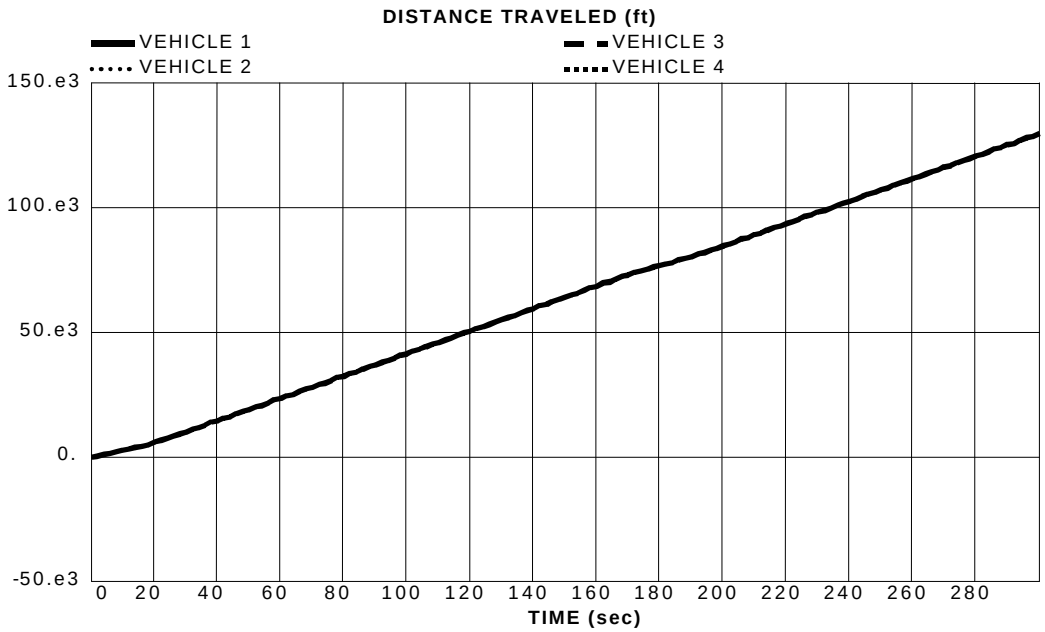

Figure 6.11 Distance traveled by four vehicles under integrated model

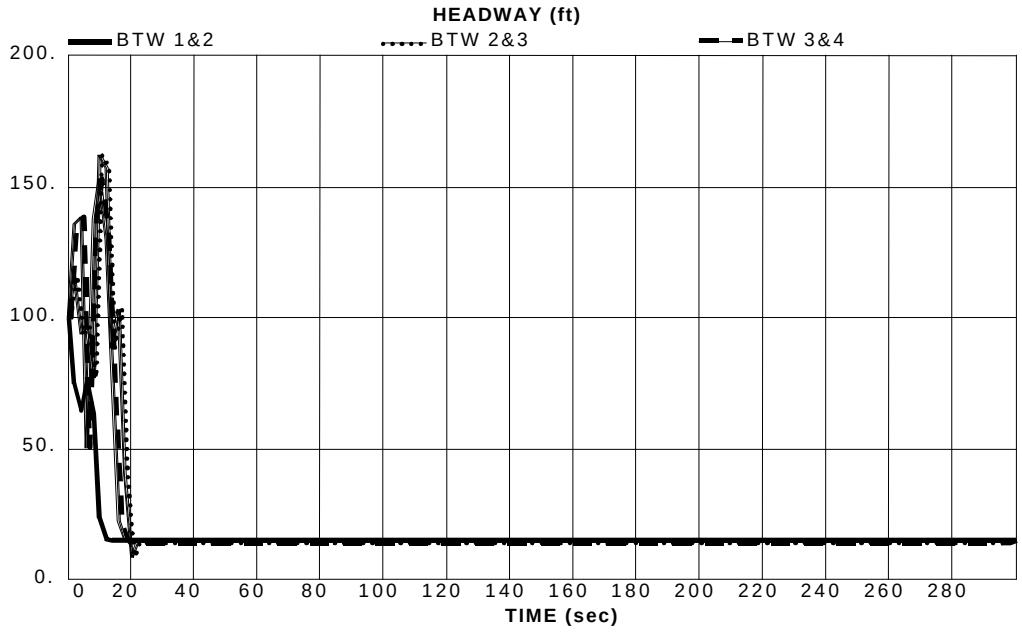

Figure 6.12 Headway between four vehicles under integrated model

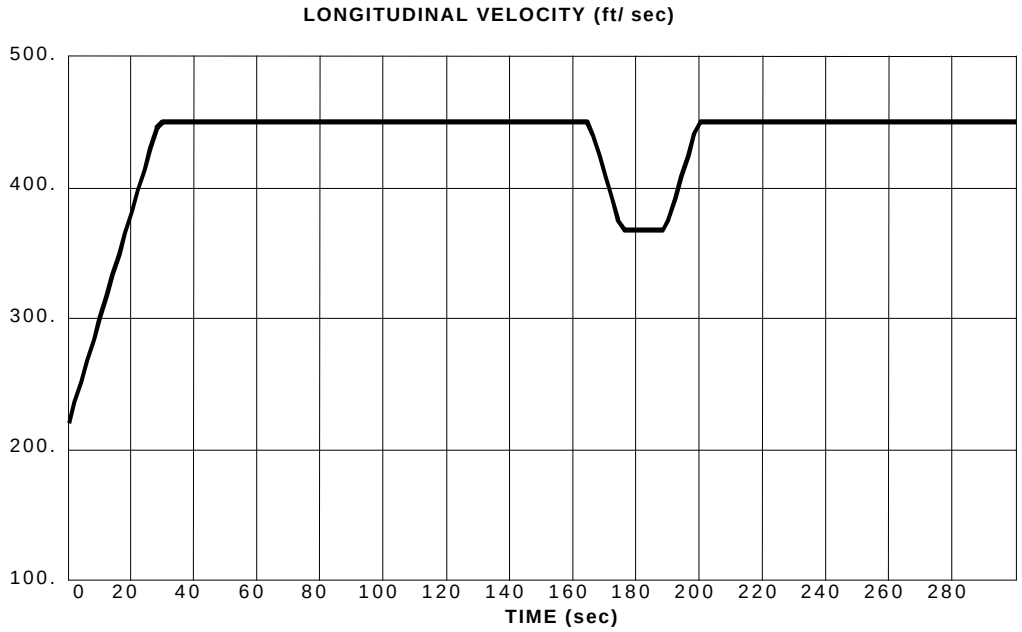

Figure 6.13 First vehicle's longitudinal velocity under integrated model

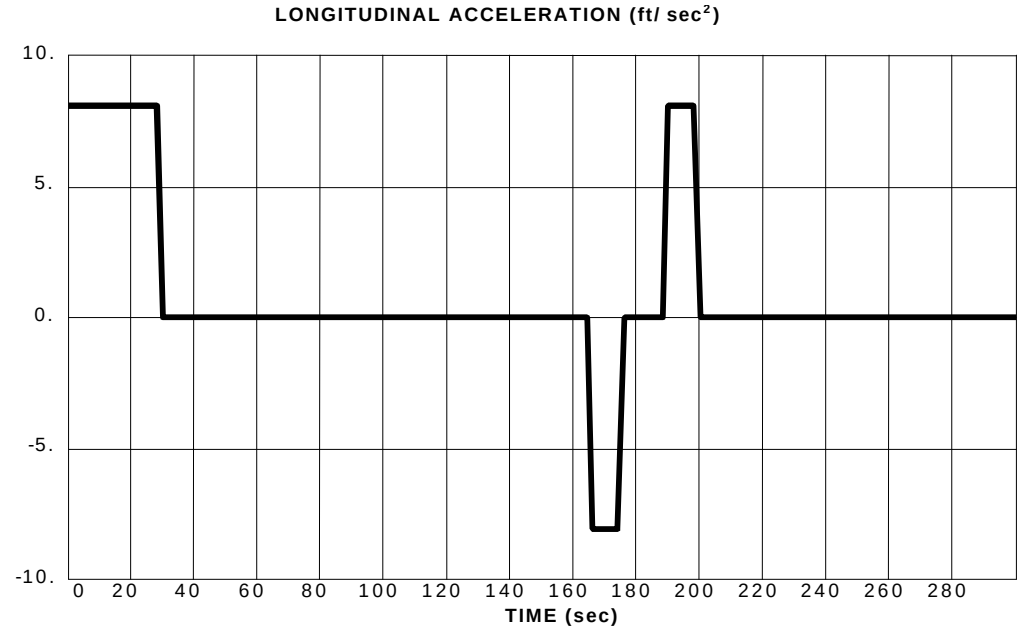

Figure 6.14 First vehicle's longitudinal acceleration under integrated model